ORNL/TM-2024/3290
S04050100-TRT10000-R01

SECOND TARGET STATION (STS) PROJECT

PIONEER Technical Report

Yaohua Liu
Peter Torres III

August 3, 2023

DOCUMENT AVAILABILITY

Reports produced after January 1, 1996, are generally available free via US Department of Energy (DOE) SciTech Connect.

Website www.osti.gov

Reports produced before January 1, 1996, may be purchased by members of the public from the following source:

National Technical Information Service
5285 Port Royal Road
Springfield, VA 22161
Telephone 703-605-6000 (1-800-553-6847)
TDD 703-487-4639
Fax 703-605-6900
E-mail info@ntis.gov
Website http://classic.ntis.gov/

Reports are available to DOE employees, DOE contractors, Energy Technology Data Exchange representatives, and International Nuclear Information System representatives from the following source:

Office of Scientific and Technical Information
PO Box 62
Oak Ridge, TN 37831
Telephone 865-576-8401
Fax 865-576-5728
E-mail reports@osti.gov
Website http://www.osti.gov/contact.html

This report was prepared as an account of work sponsored by an agency of the United States Government. Neither the United States Government nor any agency thereof, nor any of their employees, makes any warranty, express or implied, or assumes any legal liability or responsibility for the accuracy, completeness, or usefulness of any information, apparatus, product, or process disclosed, or represents that its use would not infringe privately owned rights. Reference herein to any specific commercial product, process, or service by trade name, trademark, manufacturer, or otherwise, does not necessarily constitute or imply its endorsement, recommendation, or favoring by the United States Government or any agency thereof. The views and opinions of authors expressed herein do not necessarily state or reflect those of the United States Government or any agency thereof.

PIONEER TECHNICAL REPORT		ISSUE DATE: August 3, 2023
PREPARED BY Yaohua Liu	PROJECT Second Target Station	DOCUMENT NUMBER: S04050100-TRT10000-R01

	Signature / Date					
	Rev. 00	Date	Rev. 01	Date	Rev. 02	Date
Instrument Systems Lead	Ken Herwig		Leighton Coates			
Instrument Engineering Manager	Van Graves		Van Graves			
Instr. Sys. Sci. & Technology Manager	Leighton Coates		Leighton Coates			
PIONEER Scientist	Yaohua Liu		Yaohua Liu			
PIONEER Lead Engineer	Peter Torres III		Peter Torres III			

Revision	Description
00	Initial Release
01	Replace Montel mirrors with elliptical guides and a T_0 chopper.

CONTENTS

LIST OF FIGURES

LIST OF TABLES

ACRONYMS

BT	*brilliance transfer*
CECs	*credited engineered controls*
ESS	*European Spallation Source*
FTS	*First target station*
FWHM	*Full-Width-at-Half-Maximum*
HFIR	*High flux isotope reactor*
HF	*High flux*
HR	*High resolution*
IRR	*Instrument Readiness Review*
ICS	*Integrated Control Systems*
JPARC	*Japan Proton Accelerator Research Complex*
KB	*Kirkpatrick-Baez*
ORC	*Oscillating radial collimator*
ORNL	*Oak Ridge National Laboratory*
PSI	*Paul Scherrer Institute*
QM	*Quantum materials*
RF	*radio frequency*
SCND	*Single-crystal neutron diffraction*
SiPM	*Silicon Photomultipliers*
SNS	*Spallation Neutron source*
STS	*Second Target Station*
SE	*sample environments*
SF	*Spin flipper*
TOF	*Time-of-flight*
WBS	*Work Breakdown Structure*

ABSTRACT

PIONEER is a time-of-flight single-crystal neutron diffractometer at the Second Target Station (STS), aiming at providing the world-leading capability to measure tiny crystals (~0.001 mm^3, i.e., X-ray diffraction size), ultra-thin epitaxial films (~10 nm thicknesses), and weak structural transitions and complex magnetism. The instrument will take advantage of STS source characteristics and utilize advancements in neutron optics to largely reduce the sample-volume requirement for single-crystal neutron diffraction. PIONEER will have a high-flux mode with multiple beam size options to improve the signal-to-background ratio in various sample environments. It will also provide a high Q-resolution mode by limiting beam divergence to study periodically modulated structures with characteristic lengths no less than 100 Å. Furthermore, it supports half-polarized neutron diffraction for investigating complex magnetism and local susceptibility. This report first overviews the proposed science case and the derived requirement. And then, the chosen technical solutions and expected performance will be described.

1. SCIENCE CASE

1.1 NEUTRON SCATTERING OPPORTUNITIES

Neutron scattering is an indispensable tool for understanding advanced materials. It reveals the microscopic details of the interplay among the spin, charge, orbital, and lattice degrees of freedom and their collective excitation [1]. Neutron scattering researchers are at the forefront of identifying materials that drive emerging technologies. They are dedicated to finding solutions for combating the pandemic, mitigating climate change, and tackling the increasing energy consumption of supercomputers, data centers, and artificial intelligence systems deployed worldwide. Multiple DOE BESAC reports have discussed the opportunities within these endeavors [2-6]. For example, quantum materials research holds promise for high-precision sensors, quantum computers, and secure communications [5]. At the same time, electronic materials research is crucial for faster and more energy-efficient microelectronics [4], and energy materials research will help to reduce greenhouse gases from the atmosphere for a sustainable future [2, 3]. To help US scientists seize these opportunities, we aim to provide world-leading neutron scattering capabilities.

The Second Target Station (STS) provides over 20 times or more cold neutron flux than the current world-leading First Target Station (FTS) at SNS [7]. The high peak brightness of cold neutrons and the broad wavelength band available at STS will lead to transformative capabilities, such as studying smaller samples, using sophisticated sample environments, performing time-resolved studies, and investigating hierarchical architectures in detail. New STS instruments will utilize the latest advances in neutron optics, spin manipulation, instrument design, and computational tools, enabling researchers to collect information faster and more precisely than existing instruments.

1.2 PIONEER'S CAPABLIITY AND SCIENCE CASE

PIONEER, one of the STS instruments, is a next-generation time-of-flight (TOF) single-crystal diffractometer proposed for accelerating materials research [8]. Single-crystal neutron diffraction (SCND) is a powerful structural characterization tool. SCND studies quantum magnets, superconductors, energy materials, and minerals. It provides critical and accurate microstructural information about hydrogen-related energy materials and exotic magnetic materials due to its high sensitivity to the arrangement of light elements and magnetic moments. However, neutron scattering is generally a flux-limited technique, preferring sample volume to be 1 mm^3 or larger. At the same time, there are growing demands for beamtime and sophisticated sample environments from the user community. PIONEER will be designed to fill the capability gaps to measure tiny crystals (0.001 mm^3, i.e., X-ray diffraction size), ultra-thin films (10-nm thickness), and weak structural and magnetic transitions with rapid data collection rates and sophisticated sample environments. Featured capabilities at PIONEER include:

- PIONEER provides a high-flux (HF) mode to study crystals with volumes as small as 0.001 mm^3, which is more than one-order-of magnitude lower than the current limit (~ 0.05 mm^3). It accelerates materials discovery at the early stage when large single crystals are often unavailable. Furthermore, PIONEER can probe exotic magnetic states in thin films and potentially study surface and interface states. It can also study the high-pressure induced quantum state using the commercially available x-ray diamond anvil cells.
- PIONEER features a broad wavelength band, a high Q resolution, and extensive detector coverage, increasing efficiency for time-resolved studies and measuring both Bragg reflections and diffuse

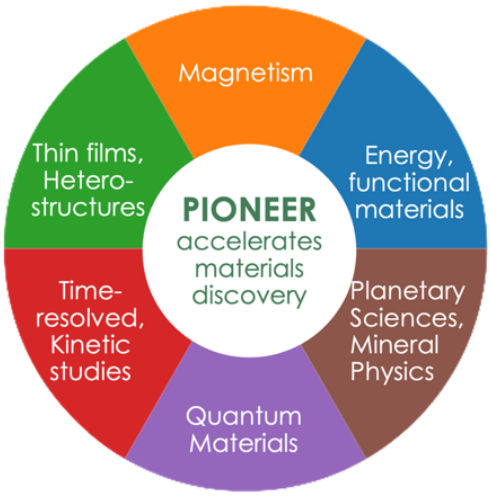

Figure 1-1 PIONEER's science scope covers a range of materials science topics.

scattering simultaneously from sub-mm^3 crystals. This will help researchers quantitively decipher crystalline samples' average and local structures.

- PIONEER supports a range of sample environments, including low/high temperatures, magnetic/electric fields, and pressure. It will enable tunable beam sizes and equips incident and scattering beam collimators to reduce the unwanted scattering from reaching detectors.
- PIONEER has a high-resolution (HR) mode to probe chemically and magnetically periodic structures with a characteristic length scale of more than 100 Å and to study large unit-cell functional materials, such as metal-organic frameworks, polyoxometalates and exotic magnetic states such as skyrmion lattices.
- PIONEER supports half-polarized single-crystal neutron diffraction that can significantly enhance the sensitivity of the atomic magnetic susceptibility.

With inputs from the user community, we have identified a broad range of research areas that can benefit from PIONEER's unprecedented capabilities [8]. As shown in Figure 1-1, they include (1) quantum materials, such as unconventional superconductivity, *4d-5d* strong spin-orbital coupling systems, and topological materials; (2) fundamental magnetism, (3) thin films and artificial heterostructures; (4) functional materials for energy, such as metal-organic frameworks, polyoxometalates, multiferroic oxides, complex hybrids, thermoelectric materials; (5) time-resolved studies, and (6) planetary sciences and mineral physics. PIONEER's science case constantly evolves with research opportunities expanding. We have recently received recommendations to study macromolecular crystals at PIONEER. PIONEER will equip a roll-in goniometer with a cryo-stream system and can be used to study macromolecular compounds using tiny crystals that are not feasible at the existing beamline.

1.3 GENERAL REQUIREMENTS FROM USER COMMUNITIES

Table 1-1 summarizes the characteristic parameters per the requirements from the science case. The sample sizes are essential to determine the optimal beam sizes. The unit-cell sizes are critical to optimizing the reciprocal space resolution, which drives the choices of the moderator-to-sample distance, the beam divergence, and the detector resolution. Almost all science cases require non-ambient experimental conditions. In the table, *T, H, P,* and *E* stand for temperatures (*T*), magnetic field (*H*), pressure (*P*), electric field (*E*), and optical pumping (*O*), respectively.

Table 1-1 Characteristic parameters collected from materials science user community.

Science case	Sample volume	Edge Length	Unit cells or supercells	Sample environments	Polarized neutrons
Quantum materials (bulk crystals)	0.001-10 mm^3	0.1 - 2 mm	3 - 100 Å	*T, H, P, E*	Yes
Interfaces, thin films, and heterostructures	Area: 2x2 to 5x5 mm^2 Thickness: 10-400 nm	2 - 5 mm	3 - 30 Å	*T, H, E, O*	Yes
Fundamental Magnetism	0.001-10 mm^3	0.1 - 2 mm	3 - 100 Å	*T, H, P, E*	Yes
Functional and energy materials	0.001-10 mm^3	0.1 - 2 mm	3 - 100 Å	*T, P, E*	No
Time-resolved studies, kinetics	0.1 - 30 mm^3	0.5 - 3 mm	3 - 30 Å	*T, H, P, O*	No
Planetary sciences and mineral physics	0.001-1 mm^3	0.1 – 1 mm	3 - 30 Å	*T, P*	No

2. INSTRUMENT REQUIREMENTS AND DESCRIPTION

2.1 INTRODUCTION

PIONEER is a next-generation time-of-flight single-crystal diffractometer at the Second Target Station (STS). The key driver for PIONEER's performance is the world-leading brightness of the STS source. Although only the coupled moderators are available at STS, the low repetition rate (15 Hz) makes building a high Q-resolution single-crystal diffractometer practical using a long source-to-sample distance.

PIONEER will harness the power of the time-of-flight (TOF) Laue single-crystal neutron diffraction (SCND) technique. The wavevector transfer Q depends on the neutron wavelength λ and scattering angle θ for the elastic scattering approximation: $Q = 4\pi \sin\theta / \lambda$. The Laue method uses a wide range of wavelengths, and modern instruments utilize area-detector arrays to measure a broad range of scattering angles. Therefore, a large volume of reciprocal space is sampled simultaneously, mapping hundreds to thousands of Bragg peaks at a single configuration, as illustrated in Figure 2-1(a). With a source-to-detector distance of 56.8 m, PIONEER will provide an effective wavelength band of ~ 4.3 Å. It will also equip an extensive detector coverage of ~ 4.2 sr, with 80° out-of-plane coverage and 260° in-plane coverage. Figure 2-1(b) shows simulated diffraction patterns on the cylinder detector from a complex metal hydride crystal $[Cu_{20}(H)_{11}\{S_2P(O^ar)_2\}_9]$ [9]. The top panel represents the scattering pattern from a 4.0-Å wavelength band, which shows numerous Bragg peaks with overlapping features, indicating the great amount of information captured by PIONEER across a broad wavelength range. The scattering data are recorded in the event mode and the contributions from neutrons of different wavelengths can be separated [10]. The bottom panel shows the data from a narrower wavelength band, where the individual Bragg peaks are well resolved. In short, PIONEER has a broad wavelength band and extensive detector coverage with minimal gaps. It enables comprehensive coverage of reciprocal space at a single crystal orientation with high Q resolutions.

The high source brilliance and the long beamline offer excellent opportunities to enhance the signal-noise ratio. We employ the best design practices and state-of-the-art neutron optics to ensure optimal performance. Benefiting from the advancements in computational tools and neutron optics, we can now design and implement optics with complex geometries. PIONEER will offer tunable beam size to reduce

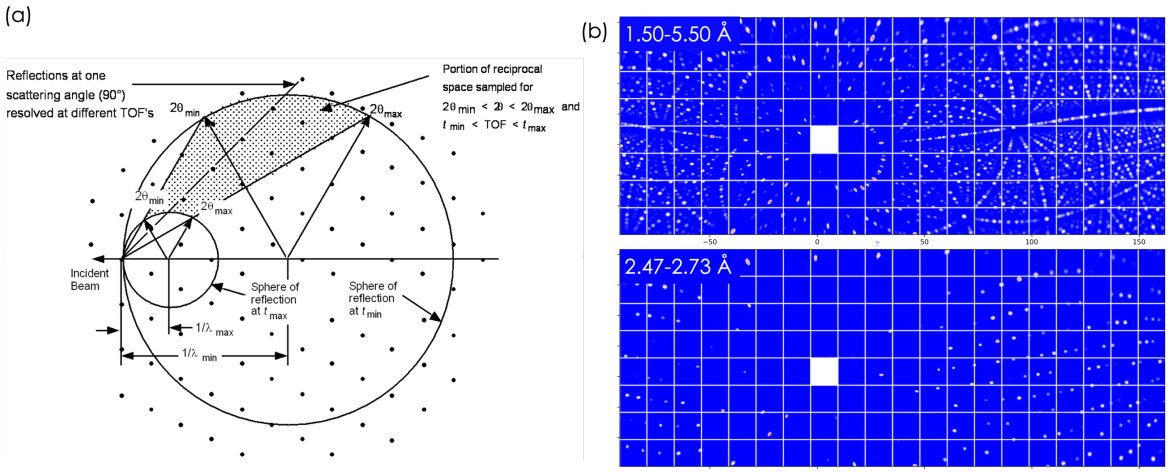

Figure 2-1 (a) Reciprocal space coverage from a single sample orientation from TOF Laue SCND with an area detector is determined by the wavelength band and the detector angular coverage. (b) Simulated diffraction patterns on PIONEER's cylindrical detector over a broad (top) and a narrow (bottom) band, respectively.

the background for tiny crystals and enable tunable divergence to improve the resolution for large unit-cell samples. To optimize its performance, we have employed the following design principles:

(1) The instrument shall deliver a high-brilliance beam to the sample position with the wavelength resolution required by the science case and remove unwanted neutrons from the incident beam as early as possible.

(2) The instrument shall provide tunable beam sizes and divergences with uniform profiles at the sample position for quantitative structural analysis.

(3) The instrument shall equip a large detector array and avoid neutrons not directly scattered by samples from reaching the detector.

(4) The end station shall accommodate the most common types of sample environments (SEs) for materials science currently used at leading neutron facilitates, particularly at the First Target Station (FTS), and shall be flexible for future upgrades.

(5) The instrument system shall enable remote operation modes and semi-autonomous experiments as reasonably achievable.

Section 2.2 will explain the instrument layout and Sections 2.3 to 2.10 will cover the instrument components by their order in the work breakdown structure (WBS). The high-level requirements for Integrated Control Systems (ICS) and scientific software are included in Section 2.11 and Section 2.12, respectively. Table 2-1 lists a summary of topics covered by each section.

Table 2-1 The covered topics.

Section	WBS index	WBS title	Comment
2.2	S.04.05.01	Technical Integration	Instrument layout
2.3	S.04.05.02	Optics	Beam characteristics, neutron transport and beam control systems
2.4	S.04.05.03	Neutron Choppers	The chopper requirement and performance
2.5	S.04.05.04	Shielding	The shielding requirement
2.6	S.04.05.05	Detectors	The detector and beam monitor
2.7	S.04.05.06	Motion Systems	
2.8	S.04.05.07	Instrument Specific	Vacuum thimble
2.9	S.04.05.08	Sample Environment	
2.10	S.04.05.09	Infrastructure & Utilities	Sample preparation and storage Utilities needs
2.11	S.06.04.05 S.06.06	Instrument Controls & DAQ Personnel Protection Systems	Integrated control systems requirement
2.12	S04.02	Scientific Software	

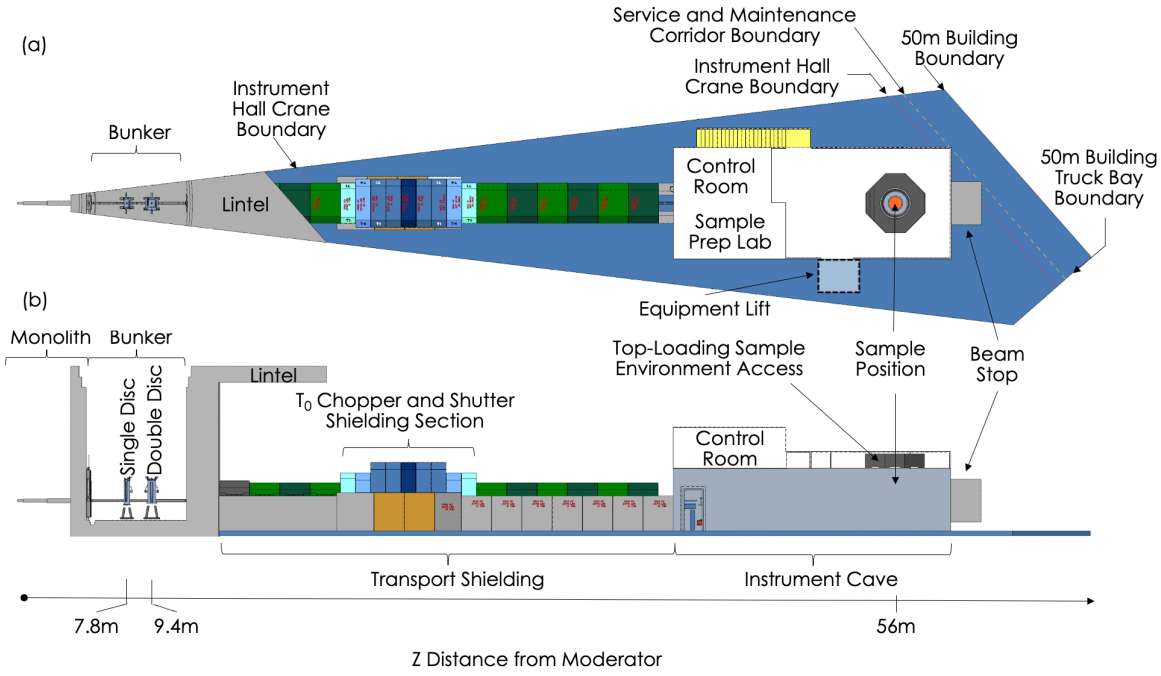

Figure 2-2 (a) plan view and (b) side view of the PIONEER instrument. The moderator locates at z= 0m. After the moderator core vessel (not shown), there are five key regions: (1) monolith, (2) bunker regions, (3) transport shielding, (4) instrument cave and (5) beamstop.

2.2 INSTRUMENT LAYOUT

Figure 2-2 shows the PIONEER instrument layout. The source-to-sample distance L_1 = 56.0 m, and the sample-to-detector distance L_2 = 0.8 m. There are five regions:

(1) the monolith with the moderator (source),
(2) the bunker with bandwidth choppers,
(3) the transport sheading from the bunker outside wall to the instrument cave,
(4) the instrument cave with the polarization system, detector, control room and sample preparation lab,
(5) a beam stop outside the instrument cave.

The detector is on the first floor of the instrument cave, and the control room and sample preparation lab are on the second floor. Top-loading sample environments will be installed from the second floor. There is an equipment lift on one side of the instrument cave.

The instrument schematic can be found in the technique report **Second Target Station (STS) Project: PIONEER Instrument Schematic** *(ORNL/S04050100-CMT10000*, version date June 2023). Figure 2-3 shows the instrument layout from the optical point of view. The polarization system, the second half-elliptical guide, and the detector are inside the instrument cave. The polarization system comprises a translatable polarizer (a multi-channel supermirror V-cavity), an adiabatic RF spin flipper, and guide-field magnets. There is a shielding wall between the polarization system and the detector to reduce the background. The end station features a vacuum timber to house top-loading sample environments, and there is an oscillation collimator between the timber and the detector.

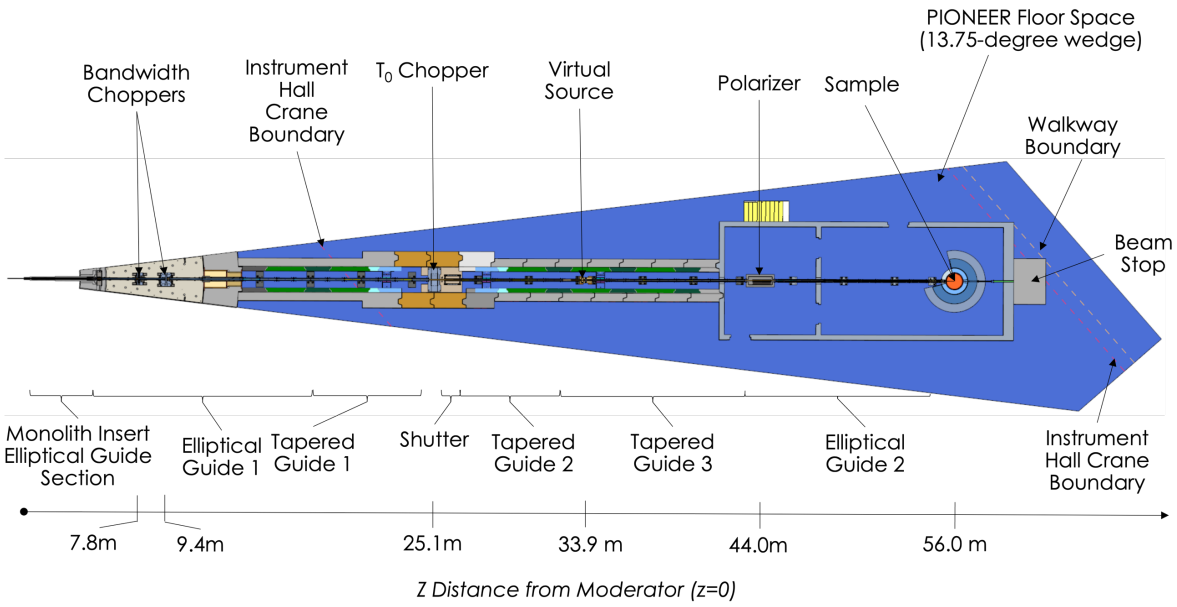

Figure 2-3 Instrument layout from the optical point of view. The guide system starts in the middle of the Monolith insert. There are a pair of bandwidth disk choppers inside the bunker. The T_0 chopper is outside the bunker wall flowing by the shutter. The is a virtual source slit at the shared focal point of the two half-elliptical guides. Inside the instrument caves are the polarization system, the second half-elliptical guide, and the detector. The beam stop starts outside the instrument cave.

Table 2-2 lists the positions of major instrument components. There are the following items by order of their distances to the moderator.

(1) The source, *i.e.*, the moderator surface, is at 0 m.
(2) The monolith insert will be filled with Helium gas and houses two optics modules. One module is a beam collimator, and the other is a portion of the guide system. The beam collimator starts at 0.948 m.
(3) The guide system consists of two half-elliptical guides connected by three tapered guides. It starts in the middle of the monolith insert at 2.588 m and ends at 54.464 m. It; however, there are multiple significant gaps in between, ranging from 0.2 to 1.9 m, to accommodate choppers, slits, monitors, and a polarization system. The two half-elliptical guides share a focal point, forming a quasi-virtual source at 34.001 m.
(4) The maintenance shield is located outside the monolith at 5.286 m. A beam collimator will be in place when the shield is inactive.
(5) The centers of 2 bandwidth choppers are located inside the bunker at 7.776 m and 9.382 m, respectively. The first is the STS large single-disk (SD) chopper to avoid frame overlap, and the second is an STS large double-disk (DD) chopper to define the wavelength band.
(6) The T_0 chopper is centered at 25.100 m to block fast neutrons, followed by a slit package.
(7) The 1.0-m long shutter is centered at 26.310 m.
(8) The instrument cave starts at 42.100 m and ends at 59.500 m.
(9) A translatable polarizing supermirror V-cavity starts at 44.050 m.
(10) The second half-elliptical guide and a fixed adiabatic radio frequency (RF) spin-flipper (SF) starts at 45.460 m. After the SF, a permeant magnetic guide field will be provided to maintain the polarization.
(11) There is a shielding wall at 47.810 m between the polarization system and the detector to reduce the background.
(12) The end station, centered at 56.000 m (sample location), includes the detector, the collimator, the

vacuum thimble, and the sample-environment supporting structure. The bottom detector array can be removed to install a roll-in goniometer system with an automatic sample changer and a cryo-stream system. The details about the end station are listed in Table 2-4.

(13) The control hutch and the sample preparation lab are on the top level of the instrument cave. The control hutch accommodates the necessary equipment and network connection to ensure the smooth operation of the instrument. The sample preparation lab includes equipment to prepare, mount, and store samples.

Other key instrument components include,

(14) The instrument shielding starts right after the bunker at 13.930 m and ends before the instrument cave at 42.100 m.

(15) There are 4 slit packages before the sample vacuum vessel to control the beam divergence and size at the sample position. A final aperture system within the thimble will have adjustable sample-to-aperture distances and tunable aperture sizes.

(16) There are 6 beam monitors for diagnostic purposes. These monitors are translatable and remain outside the beam during operation, except for the last one that shall stay in place during operation.

(17) There are 23 Al windows to break the neutron transportation system into separated environmental control sections, either with He gas (1.1 bar for monolith insert and maintenance shield) or in rough vacuum ($< 5x10^{-3}$ mbar pressure, all others).

(18) There are 4 incident beam collimators along the guide system to block unwanted neutrons. There is an additional one insider the polarization vessel when the polarizer is not in place.

Table 2-2 Major optical components and their locations. The distance from moderator Z is measured at the starting position of the component unless specified.

Component	Description	Distance from Moderator
moderator	Port 11	Z = 0.000 m
Monolith insert widow, at Z = 0.933 m		
beam collimator 1	L = 1.640 m, coarse	Z = 0.948 m
elliptical guide 1-1	L = 2.658 m	Z = 2.588 m
Monolith insert widow, at Z = 5.253 m		
maintenance shield	Input-output window L = 0.226 m	Z = 5.360 m (center)
beam collimator 2	L = 0.208 m, coarse, in place when shield is inactive.	Z = 5.294 m
elliptical guide 1-2	L = 2.0 m	Z = 5.584 m
beam monitor 1	translatable	Z = 7.707 m (center)
single disk chopper, SD1	large SD, D=1.24 m, 15 Hz	Z = 7.776 m (center)
elliptical guide 1-3	L = 1.5 m	Z = 7.819 m
double disk chopper, DD2	large DD, D=1.24 m, 15 Hz	Z = 9.382 m (center)
beam monitor 2	translatable	Z = 9.561 m (center)
elliptical guide 1-4	L = 1.915 m	Z = 9.592 m
Bunker wall window at Z= 11.520 m		
elliptical guide 1-5	L = 2.383 m	Z = 11.528 m
Bunker wall window at Z = 13.918 m		
elliptical guide 1-6 /tapered guide 1	L = 11.000 m	Z = 13.926 m
T_0 chopper	Input-output window L = 0.598 m	Z = 25.100 m (center)
slits 1		Z = 25.695 m (center)
shutter	L = 1.000 m	Z = 25.810 m
tapered guide 2	L = 6.000 m	Z = 26.834 m
beam collimator 3	L = 1.000 m, coarse,	Z = 32.834 m
slit 2		Z = 34.001 m (center)
beam monitor 3	translatable	Z = 34.195 m (center)
tapered guide 3	L = 9.000 m	Z = 34.571 m
Instrument cave wall starts at Z = 42.100 m		
beam monitor 4	translatable	Z = 43.940 (center)
Polarizer vessel	translatable, a polarizing V-cavity and a coarse collimator	Z = 44.050 m
elliptical guide 2	L = 9.000 m	Z = 45.460 m
spin flipper	radio frequency	Z = 45.460 m
guide field	L > 8.5000 m	Z = 45.960 m
Shielding wall starts at Z = 47.810 m		
slit 3		
beam monitor 5	translatable	Z = 54.800 m (center)
beam collimator 5	L = 0.436 m	Z = 54.871 m
slit 4		Z = 55.370 m (center)
Sample location at Z = 56.000 m		
beam monitor 6	fixed	Z = 57.400 m (center)
get-lost tube		Z = 57.407 m
Instrument cave wall ends at Z = 59.500 m		
beam stop	Starts after the wall	Z = 60.450 m (center)

Table 2-4 Key components at the end station. R is the radial distance, and Y is the vertical displacement with respect to the nominal sample location.

Component	Description	R and Y from the sample position (mm)
sample location		(0, 0, 0)
vacuum thimble	cylindrical with extended collimator tubes in the direct beam direction.	R = 506 (out)
vacuum valve		R = 521 (center)
radial collimator	oscillating, gauge length < 40 mm absorbing blade, R = 525-775 mm supporting structure, R = 518-782 mm	R = 650 (center)
vertical detector array	4.2 sr, SiPM anger camera, a cylindrical array with an oscillating radial collimator In-plane coverage: -160° to +98° out-of-plane coverage: of -36° to +47°	R = 800.0
bottom detector array	0.4 sr, SiPM anger camera, a flat array with a cone collimator	Y = -800.0

Table 2-3 Preferred incident beam characteristics at the sample location.

Beam parameters	Values	Comments
minimum accessible wavelength range	1.0-6.0 Å	Q range: 0.2 – 12.5 Å^{-1}
highest resolution, dQ/Q	≤ 0.3%	near backscattering
wavelength band width	≥ 4.0 Å	selected by the bandwidth chopper
beam divergence (FWHM)	high flux mode: ≥ 0.6º high resolution mode : ≤ 0.3º	controlled by slits
beam size with a high homogeneity	1×1 mm^2 (min.) to 5×5 mm^2 (max.)	controlled by slits and final aperture
For polarized incident beam only		
minimum wavelength	≤ 1.5 Å	Q range: 0.2 – 8.0 Å^{-1}
Polarization	≥ 90%	@ 1.5 Å^{-1}

2.3 OPTICS (WBS S.04.05.02)

2.3.1 Required incident beam characteristics

We have derived the beam characteristics from the science requirements and technical constraints, as listed in Table 2-3 to guide the instrument design.

The minimum wavelength λ_{min} of 1.0-Å is derived from the preferred real-space resolution. The minimum wavevector transfer, Q_{min}, is driven by the long periodicity of chemically and magnetically modulated structures. The wavelength bandwidth is determined by the source frequency, neutron emission profile, and chopper setting λ_{max} of 6.0-Å requirement is less strict and driven by λ_{min} and the available bandwidth.

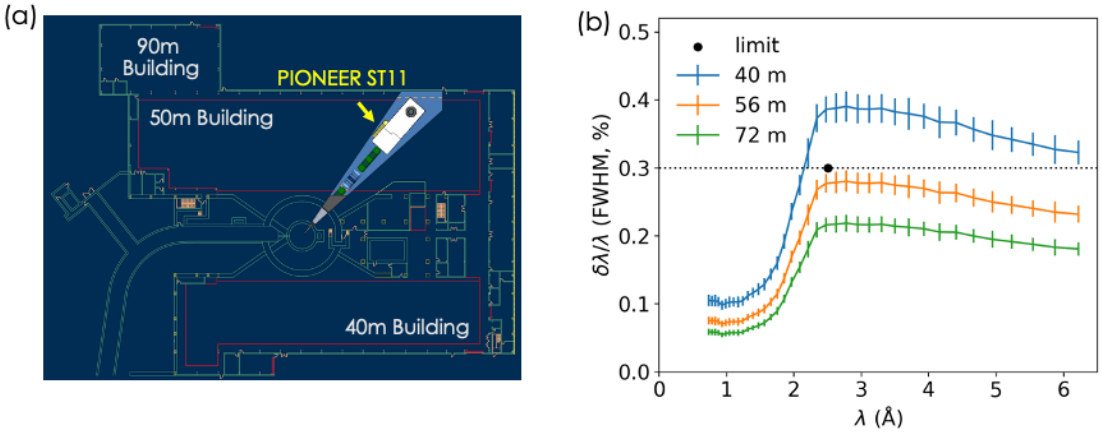

Figure 2-4 (a) PIONEER will be located at ST11 inside the STS building. (b) The wavelength resolution as a function of the moderator-to-sample distance L_1.

The wavelength resolution $d\lambda/\lambda$ shall be better than 0.3% for the available wavelength range. This enables the required high Q resolution to study large characteristic lengths of chemically and magnetic modulated structures to 100 Å or more. The $d\lambda/\lambda$ is the ratio between the emission time (FWHM) and the total time-of-flight for neutrons transported from the moderator to the detector. With the known time structure of the emitted neutron pulse, the required $d\lambda/\lambda$ determines the minimum source-to-sample distance ($L_{source\text{-}sample} = L_1+L_2$). shows the wavelength resolution for different moderator-to-sample distances L_1, estimated from Monto-Carlo simulations. The sample-to-detector distance is fixed to be 0.8 m. The calculation uses the moderator source file of *ST-13-CY46D-MID-March_2022.dat* (from Igor Remec). PIONEER will extract the beam from the upper pure-parahydrogen cylindrical moderator that provides a narrower neutron pulse width for a better wavelength resolution than the bottom tube moderator [7]. The cylindrical moderator requires a shorter beamline length for a fixed wavelength resolution, providing a broader bandwidth. As shown in Figure 2-4, with L_1 = 56.0 m, PIONEER achieves $d\lambda/\lambda$ better than 0.3% over 1.0-6.0 Å, matching the resolution requirement. The beam port ST11 is chosen for PIONEER so that it will face the cylindrical moderator and remain within the STS 50-m building.

The maximum wavelength bandwidth can be estimated from $L_{source\text{-}sample}$ and the pulse frequency, which is 4.64 Å for PIONEER. Due to the finite pulse width, we will achieve a slightly narrower bandwidth, ~ 4.3 Å. The beam divergence and size shall be tunable for different experiment needs. The beam divergence for the high-flux (HF) mode is comparable to the typical crystal mosaic, defined by the full width at half-maximum (FWHM). The high-resolution mode requires a narrower divergence. PIONEER will mostly study sub-mm size crystals for structural determination and will use large samples for thin-film experiments, time-resolved studies, and pulsed-field studies. The extensive detector coverage is critical for experiments with tiny samples and rapid data collection. The beam size is defined by a region with uniform flux distribution. The beam profile within this region shall be uniform to reduce systematic errors, and the flux outside this region shall be low to reduce background.

A polarized incident beam is required for local magnetic susceptibility studies, where λ_{min} *of* 1.5 Å is needed to reach a Q_{max} of 8.0 Å^{-1}. The incident beam polarization shall be > 90% for neutron wavelength as shorter as 1.5 Å, and the transmission rate shall be > 35%.

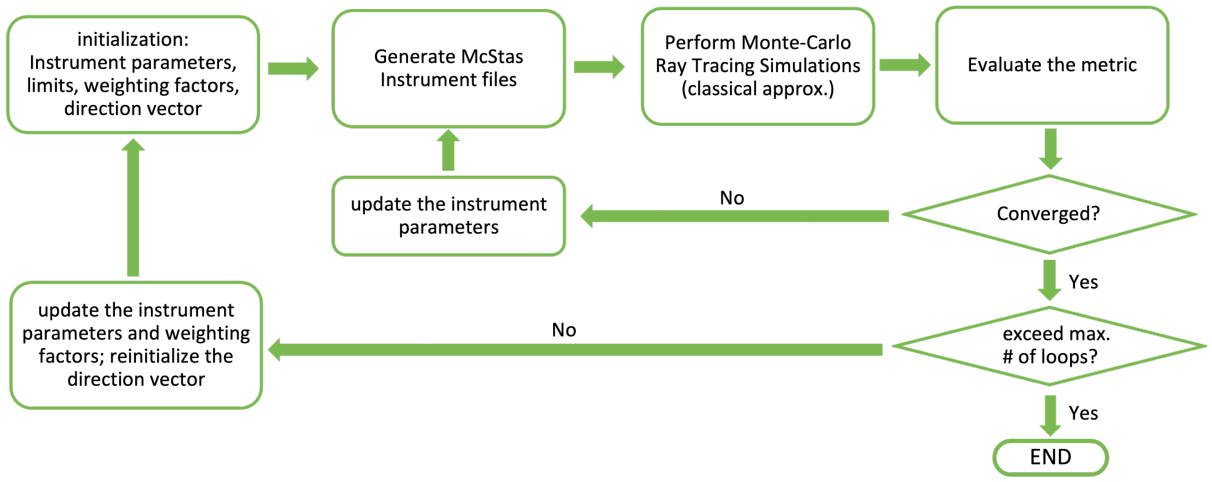

Figure 2-5 The numerical optimization workflow for the guide geometry.

Overall, the neutron optics system shall transport neutrons from source to sample position (56.0 m) over the entire wavelength range (1.0-6.0 Å) with a uniform illumination area of 5×5 mm^2 and a divergence range of more than ±0.3° in both horizontal and vertical directions, which represents the maximum phase space required by PIONEER's science case. The angular and spatial distributions of the beam profile shall be as homogeneous as reasonably achievable. Bandwidth choppers shall select a > 4.0-Å band, and a slit system shall control the beam size and divergence as needed.

2.3.2 Neutron transport and beam control system optimization

Advancements in computational tools and neutron optics have enabled us to design and implement neutron transport and beam control systems with complex geometries. Figure 2-5 shows the workflow of the numerical optimization process. The essential aspect of our optimization process is choosing the metric,

$$metric = I_{roi} - \left(w_0 \times I_{outside-div-roi} + w_1 \times I_{outside-spatial-roi}\right) - \left(w_2 \times STD_{div-roi} + w_4 \times STD_{spatial-roi}\right) - R(cost) - R(slit\_eff)$$

I is the intergraded flux, STD is the standard deviation, and w_0-w_4 are the hyperparameters to control weighting factors for the undesired flux and flux fluctuation. Note that the metric is evaluated in a four-dimensional phase-space ROI. The typical spatial and angular grid sizes are 50-200 μm and 0.02-0.04°, respectively. We have decoupled the spatial and angular degrees of freedom for the (w_0-w_4) terms. *R(cost)* and *R(slit_eff)* are regularization functions that consider the mirror cost and the slit efficiency. *R(cost)* is typically ignored during optimization. *R(slit_eff)* is a function of unwanted flux removed by the slit system. The metric reflects the three objectives of the neutron transportation and beam control system for PIONEER: (1) to deliver a high-flux beam within the region of interest to maximize the signal, (2) to remove unwanted neutrons from the beam as early as possible to minimize the background, and (3) to provide a uniform beam to reduce systematic errors during measurements.

After an extensive study comparing four different guide types, we have confirmed that a straight beamline geometry is the best option for PIONEER's science case. The details can be found in Appendix A. A straight beamline provides high fluxes for both thermal and cold neutrons but requires a T_0 chopper to eliminate the high-energy neutron and gamma radiation from the moderator.

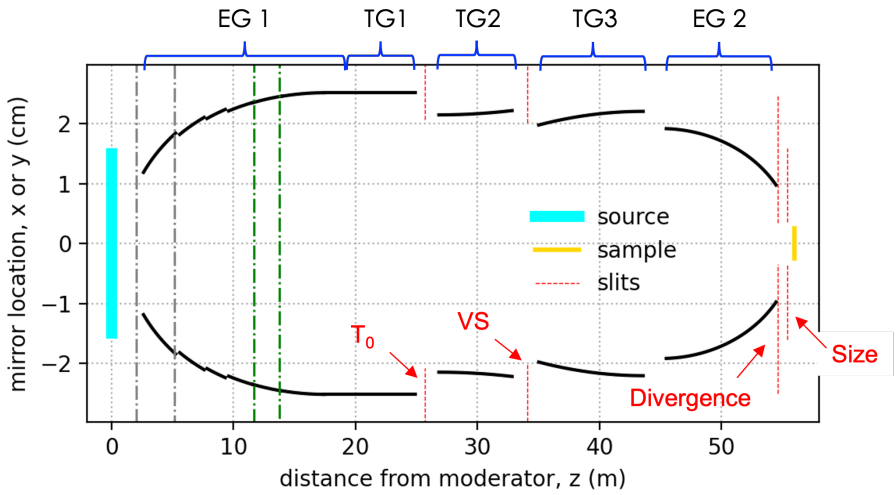

Figure 2-6 The locations of the supermirror surfaces (black curves). The guide has a symmetric geometry between the horizontal and vertical directions. The mirror elements are grouped into 5 different sections. EG stands for elliptical guide, and TG stands for tapered guide. The locations of the four slit packages are shown by the dashed red lines. The gray and the green dot-dashed lines label the monolith and the bunker walls.

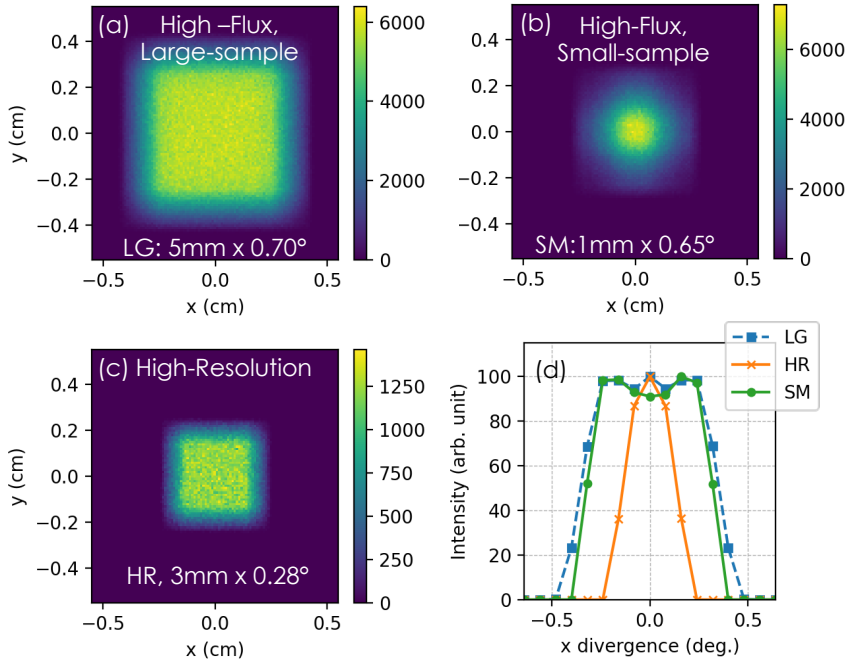

Figure 2-7 (a)-(c) The spatial beam distribution when the desired beam sizes are 5x5 mm² (HF-LG), 1x1 mm² (HF-SM) and 3x3 mm² (HR), respectively. (d) The angular distribution of the beam profile for the three cases, showing FWHMs of 0.70°, 0.65° and 0.28°, respectively.

The numerical optimization and data analysis software packages include McStas [11, 12], MCVine [13, 14], SciPy [15], and JupyterLab [16]. The Monte-Carol ray tracing simulations have considered several guide imperfections, gravity effects, and technical constraints. The McStas component Guide_gravity() is used. We have used a reflectivity slope value α =3.044 Å and a wavy value of 0.0057^{o} ($1x10^{-4}$ rad) (see Appendix A.8 and Appendix B for more information). The guide contains multiple significant gaps along the neutron guide system, from 0.2 to 1.9 m for choppers, slits, monitors, and a polarization system. Truly curved guides are avoided because of technical concerns and cost. Instead, we use polygon-approximated curved guides. As vendors suggest, individual mirror element length is limited to 0.5 m or shorter.

Figure 2-6 shows the optimized guide geometry. The chosen guide system consists of two half-elliptical guides with a shared focal point in the middle of the guide, the two half-elliptical guides are connected by three tapered guide sections. Compared to the conventional single ellipse design, this new design reduces the maximum cross-section of the guide. The guide has a square cross-section centered at the nominal beam center (x=y=0). The gravity effect is very weak for the wavelength band of interest; therefore, the guide has a symmetric geometry between the horizontal and vertical directions. Also shown in the figure are the source surface and the locations of the nominal sample location and the four slit packages: (1) one between the T_0 chopper and the shutter, (2) one at the shared focal point of the half-elliptical guides, (3) one right after the end of the guide and (4) one right before the vacuumed valves. Like TOPAZ and Mandi, PIONEER will use a final beam collimator before the sample (not depicted here).

The slit packages are used for the beam size and divergence control for different experimental needs. The optimal numbers and locations of the slit packages have been carefully investigated. The optimization has considered three specific cases simultaneously, *i.e*, (1) high-flux and large sample (HF-LG), (2) high-flux and small sample (HF-SM), and (3) high resolution (HR). Figure 2-7 shows the beam profiles for the three cases. Three instrument files are generated with identical guide geometry parameters for each optimization iteration but have different slit settings. The instrument will be evaluated for its own metric for the chosen ROIs, and the guide geometry optimization will use the combined metric.

2.3.3 Supermirror coating optimization

We have estimated the mirror-element-dependent m-coating requirement. As mentioned in APPENDIX B, supermirrors with an m-coating value up to 8 are commercially available. However, high m-value supermirrors cost significantly more and show a higher drop in reflectivity at the low-Q range. Therefore, the best option is to choose the lowest m-values required by the science case.

Figure 2-8 shows the workflow to determine the mirror element-wise m-coating profile. An instrument file with a uniform m-coating profile with m = 6 was generated. Then we perform Mont-Carlo ray tracing simulations and save all the details about individual mirror reflection, including the ray index and wavelength, the reflection index, the mirror element index, and the reflection location and angle. Using the neutron beam information collected at the sample locations, we filter the neutron rays by a chosen ROI. This ROI includes limitations on the spatial and angular distributions, the wavelength range, and weights. Neutron rays with low weights are excluded. Among the three cases, the HF-LG case requires the highest m-value supermirrors, determining the ROI to filter the favored neutrons. At the same time, we have chosen λ_{cutoff} = 1 Å, as required by the science case. The guide will transport neurons with shorter wavelengths, but the neutron transport efficiency will significantly reduce.

Figure 2-9 show the optimized m-value profiles of the supermirror coating, which have m-values ranging between 1.0 and 3.5. As expected, the m-values are higher at locations with higher local curvatures, i.e., at both ends of the guide system.

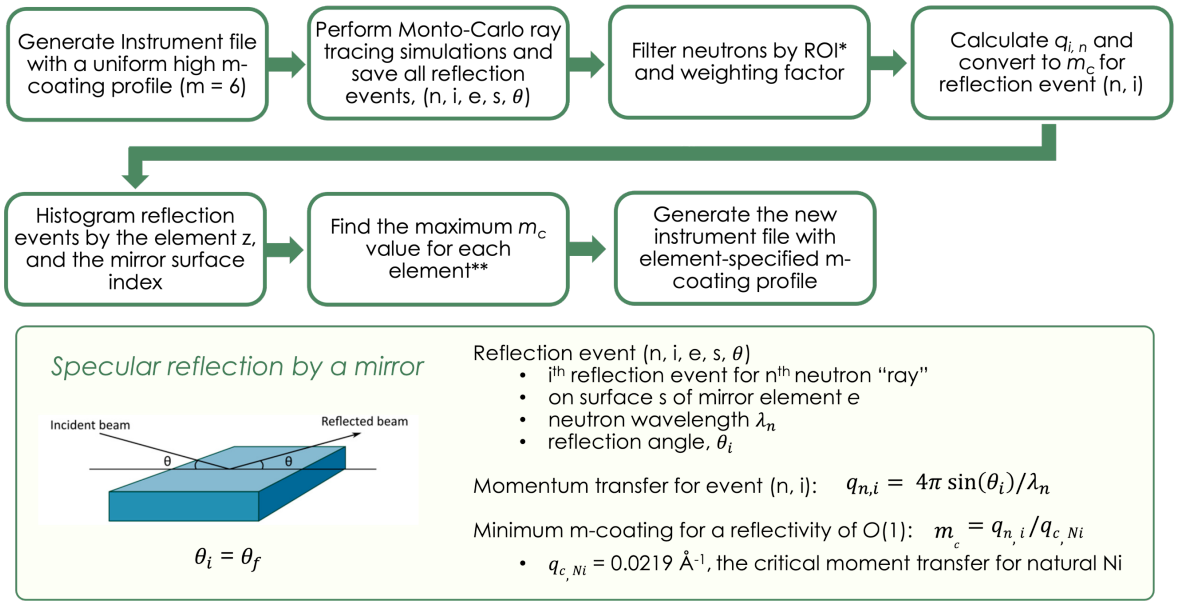

Figure 2-8 Workflow to determine mirror element-wise m- profile.

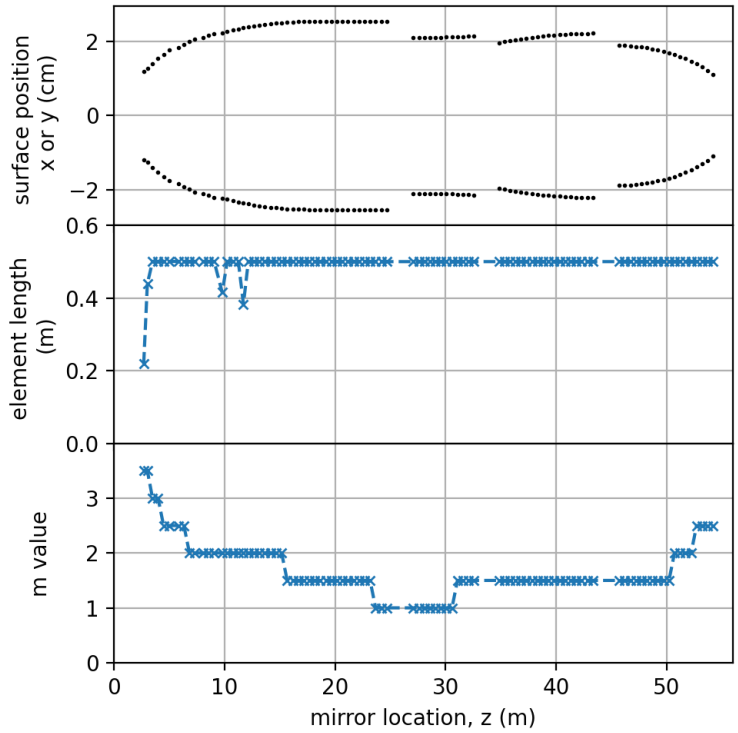

Figure 2-9 (a) The mirror surface location, (b) the mirror element length and (c) the optimized element-wise m-value.

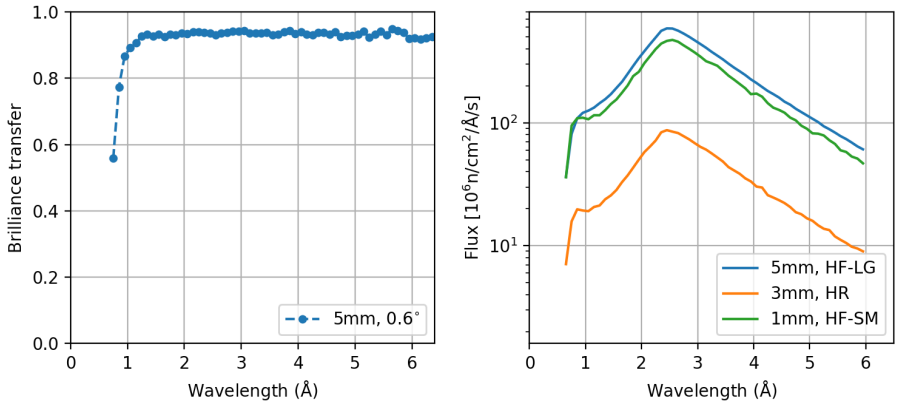

Figure 2-10 Brilliance transfer and flux at the sample position. The brilliance transfer is evaluated over the phase space of 5x5 mm² and the ±0.3° divergence using the HF-LG mode. The fluxes are evaluated over 5x5 mm², 3x3 mm· and 1 x1 mm² for the HF-LG, HR, and HF-SM modes, respectively.

2.3.4 Neutron transport performance

The neutron transport efficiency is evaluated from Brilliance transfer, which quantifies the ratio of the beam brilliance at the sample location relative to the source brilliance. With a maximum possible value of one, brilliance transfer is an excellent metric to evaluate the system's performance. The beam homogeneity is evaluated by analyzing multiple two-dimensional slices in the phase space. Mirrors' misalignment effects have not been included here and are discussed in Appendix A-. At the same time, the attenuation along the beam path due to the Al windows or air scattering has been ignored.

Figure 2-10 shows the simulated brilliance transfer (BT) and the flux at the sample position. The brilliance is assessed over a square region of 5x5 mm² and the ±0.3° divergence range along with horizontal and vertical directions. The BT value is about ~ 93% for neutrons with wavelengths between 1.3-6.0 Å. It gradually decreases as wavelength decreases, reaching 88% for 1.0-Å neutrons, and quickly decreases as the wavelength decreases further. The initial slow reduction is due to the increased wavevector transfers for shorter-wavelength neutrons on reflection, and the reflectivity decreases above q^{Ni} (see Appendix B for more information). The rapid BT reduction below 1.0-Å is because $\lambda_{cutoff} = 1$ Å has been chosen to optimize the supermirror coating profile.

The fluxes are evaluated for three cases, with a spatial ROI of 5x5 mm², 3x3 mm· and 1 x1 mm², respectively. The wavelength-dependent flux profiles peak at 2.5 Å, the same as the source brilliance. The wavelength-integrated fluxes are evaluated from a 4.3-Å wavelength band, which the bandwidth chopper will select. The values are listed Table 2-5.

Table 2-5 Estimated peak flux and wavelength integrated flux from a 4.3-Å wavelength band at the sample position.

Mode	**ROI**	Peak flux, *2.5 Å* (n· Å^{-1} cm^{-2}·s^{-1})	Integrated flux (n·cm^{-2}·s^{-1})	
			[0.8-5.1] Å	*[1.7-6.0] Å*
HF-LG	5×5 mm²	5.8 ×10^8	12.26 ×10^8	11.70 ×10^8
HR	3×3 mm²	0.87 ×10^8	1.81 ×10^8	1.72 ×10^8
HF-SM	1×1 mm²	4.7 ×10^8	9.86 ×10^8	9.34 ×10^8

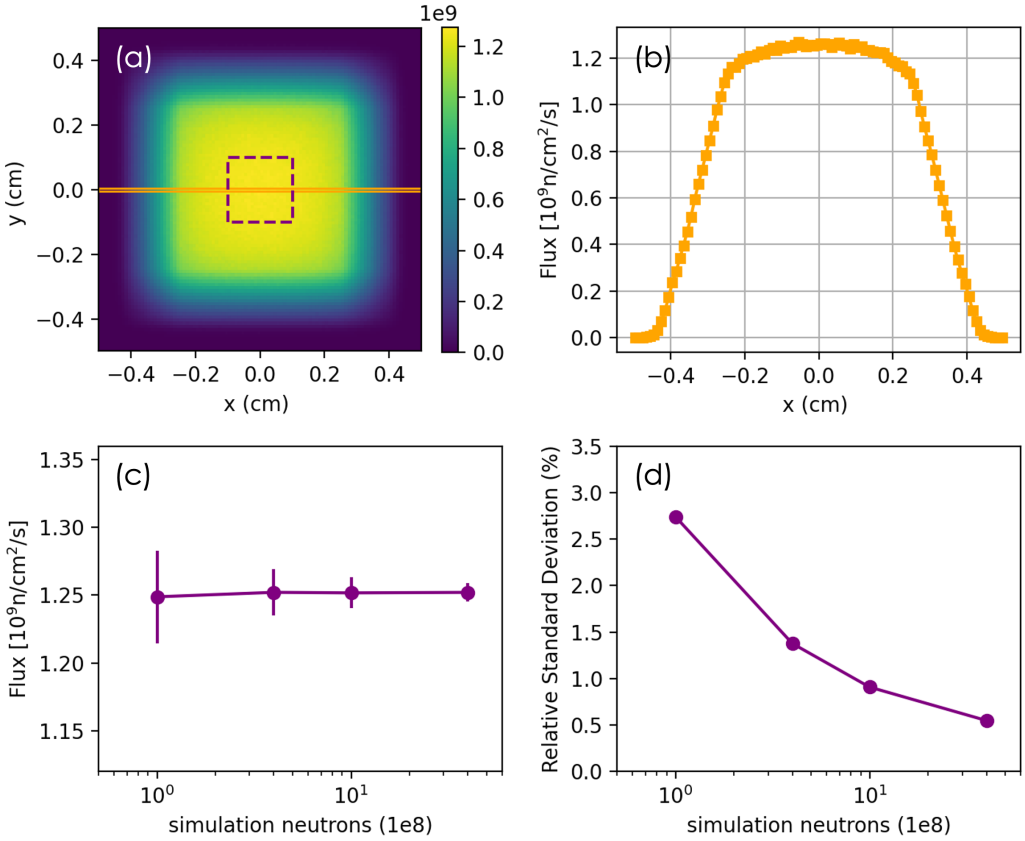

Figure 2-11(a) wavelength(a) wavelength-integrated beam profile for the HF-LG mode showing a uniform region of 5×5 mm^2. (b) the line profile along the x-direction of the flux integrated within y=[-50 μm, 50μm] at the nominal beam center. The boundary is shown by the orange lines in panel (a). (c) Average flux and STD over a 2×2 mm^2 region (the purple dashed box in panel a) at the nominal beam center estimated using a bin size of 100×100 μm^2, as a function of number of simulated neutrons, which shows that the ideal guide system delivers a highly homogenous beam, and the observed flux variation is dominated by the statistics.

The optimized guide system delivers a highly homogeneous beam at the sample position. Figure 2-11 (a, b) shows the beam profile and the line cuts for the HF-LG mode. The relative standard deviation decreases as the number of neutrons in the simulation increases, indicating that the observed flux variation is largely from the statistics from the Monto-Carlo simulations. Overall, without considering the guide misalignment effect, the spatial flux variation shows a relative standard deviation of less than 0.6%

2.3.5 Beam control performance

As mentioned earlier, PIONEER will use four piezoelectric slit packages (https://www.jjxray.dk/p/neutron-slits/) to control the beam size and divergence at the sample position in horizontal and vertical directions: (1) a T_0 slit, (2) a VS slit, (3) a divergence slit, and (4) a size slit. As shown in Figure 2-7, the slit packages give rise to spatially homogeneous beam profiles and reduced flux outside the required ROI.

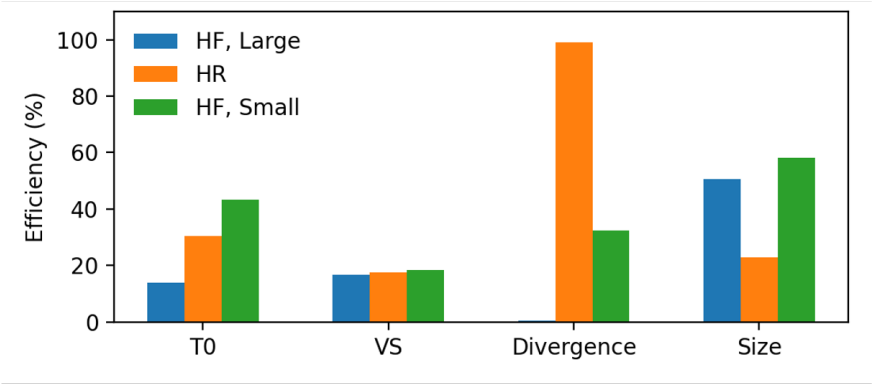

Figure 2-12 The effectiveness of the slit packages in removing unwanted neutrons from the incident beam for three different modes. The slit system uses different settings for different modes.

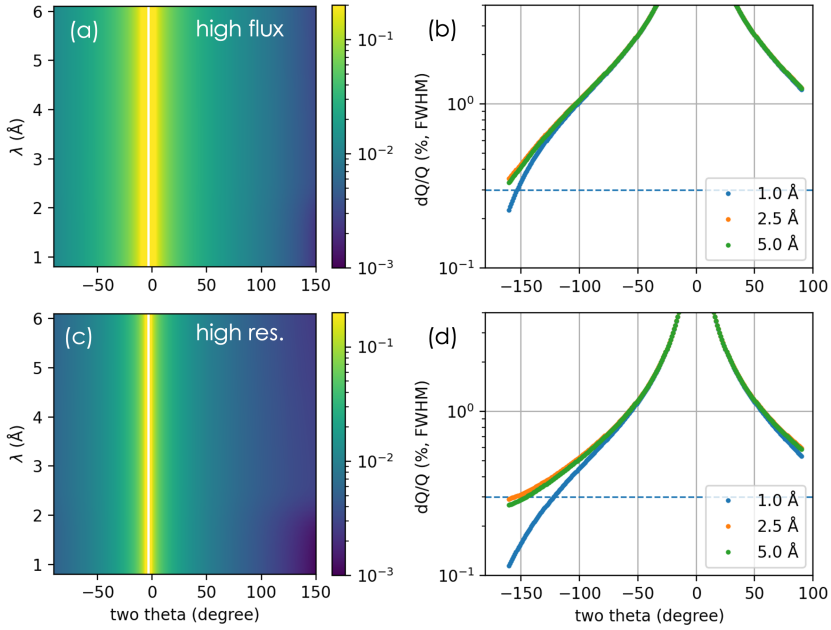

Figure 2-13 Wavelength-dependent instrument relative Q resolution (FWHM) for (a, b) the high flux mode (beam divergence FHWM = 0.70°) and (c, d) high-resolution (beam divergence FHWM = 0.28°).

A primary goal of beam control is to eliminate unwanted neutrons from the incident beam as early as possible, thereby reducing background. The effectiveness has been quantified by the percentage of incident flux outside the region of interest (ROI) eliminated by each slit using a simple metric,

$$\eta = 1 - \frac{I_{post-slit} - I_{roi}}{I_{pre-slit} - I_{roi}}.$$

$I_{pre\text{-}slit}$ and $I_{post\text{-}slit}$ are the integrated flux before and after a slit, and I_{roi} is the integrated flux within the spatial ROI at the sample location. If a slit fails to remove any neutrons from the beam, the flux before and after the slit will be unchanged, yielding zero efficiency. Conversely, suppose the flux after the slit is equal to the flux within the requested region of interest. In that case, the slit has successfully removed all unwanted neutrons, resulting in an efficiency of 100%. Figure 2-12 shows the effectiveness of the slit system in removing unwanted neutrons from the incident beam for three different operational modes. Note that the third slit is highly efficient for the high-resolution mode by reducing beam divergence, and the last slit is most efficient for small samples. Hence, the two slits are called the divergence and size slits.

The slit system also reduces beam divergence for a better Q resolution. The instrument resolution (FWHM) has been calculated from the beam divergence, the detector angular resolution, and the wavelength resolution as a function of the scattering angle (2θ) and wavelength (λ), using the following equation,

$$(\frac{dQ}{Q})^2 = \left(\frac{d\lambda}{\lambda}\right)^2 + (\cot(\vartheta)d\vartheta)^2,$$

where $d\theta$ has contributions from both the beam divergence and detector angular resolution and the sample contribution has been ignored.

$$(d\vartheta)^2 = (d\vartheta_{beam})^2 + (d\vartheta_{detector})^2,$$

$d\theta_{beam}$ = 12.2 mrad (0.7°) and 4.9 mard (0.28°) for the HF and HR modes, respectively. $d\theta_{detector}$ = 0.75 mrad (0.6 mm resolution). The results are shown in Figure 2-13. As expected, the Q resolution is dominated by the angular resolution, particularly at low 2θ angles. However, dQ/Q becomes less than 0.3% at high angles for short wavelengths (λ < 2.1 Å) for the HF model and for the entire wavelength band for the HR mode.

We have performed a virtual experiments on the using the HR mode and a wavelength band of 0.9-6.0 Å from a fake simple cubic lattice with a lattice constant of 100 Å, as shown in Figure 2-14. The Bragg peaks are well separated in the entire reciprocal space. Therefore, using the HR mode, PIONEER will be able to study large unit cells with lattice constant at least to 100 Å.

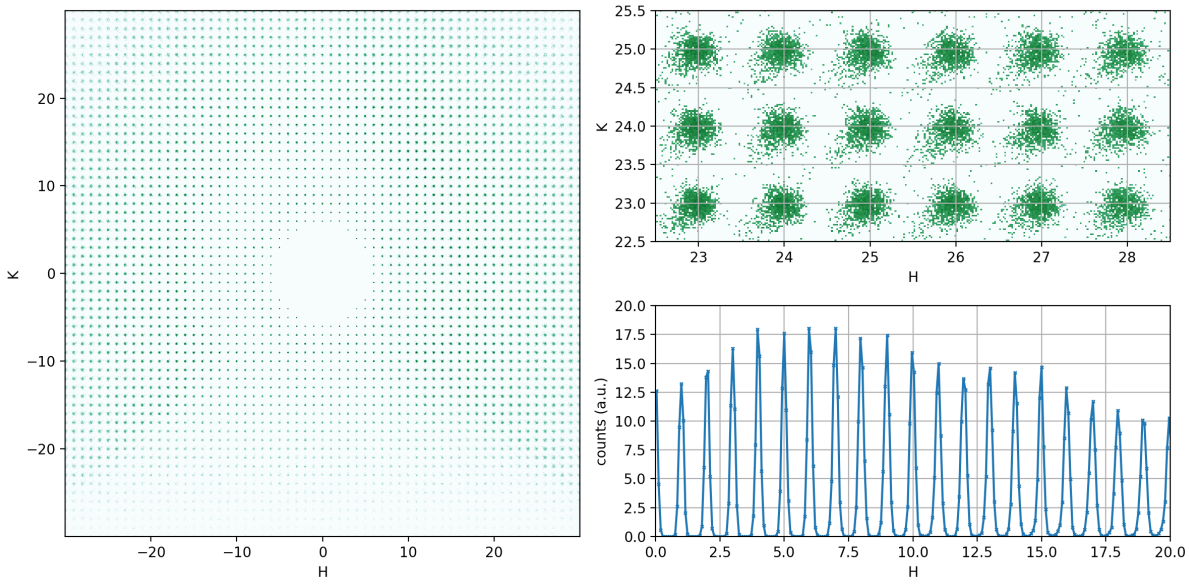

Figure 2-14 Simulated diffraction pattern using the HR mode from a fake simple cubic lattice with a lattice constant of 100 Å. Each unit cell has one Si atom, and the crystal has mosaics of 0.3°, the incident beam is along the [0 0 1] direction. 2D slices in the HK0 plane (a) over a large reciprocal space and (b) over a small region, where the signals are integrated over the full L range. (c) A line cut along the [H, 0, 0] direction. The signal is integrated over K = [23.5, 24.5], and L = [0, 40].

2.3.6 Polarization system

The PIONEER's polarization system consists of a translatable polarizing V-cavity [17], a fixed adiabatic radiofrequency neutron resonant spin-flipper [18], and a permanent guide field. The translatable polarizer locates before the second elliptical guide. A radiofrequency adiabatic spin-flipper will be placed around the beginning part of the second elliptical guide to reverse the spin polarization.

We have simulated the non-polarized beam's flux distribution at the polarizer's entrance to optimize the V-cavity, as shown in Figure 2-15. We filter neutrons based on a selected region of interest similar to what we have used to determine the supermirrors' m-coating profile. Here, we have only considered neutrons within a spatial region of interest is 5×5 mm^2 at the sample location with a significant weight, however neutrons with all divergences are considered. Due to gravity effects, the y-direction show an asymmetric angular distribution with a slightly larger range. Since a broader angular distribution requires a higher m coating, using vertical polarizing mirrors to reflect neutrons in the x-z plane is advantageous. This allows the neutron beam to be polarized along the vertical direction (y) after the polarizer. After considering the beam size at the polarizer location and the polarizer's alignment requirement, we have chosen the V-cavity cross-section to be 4.6 × 4.6 cm^2.

The typical metric to evaluate the performance of a polarizer is $\mathbf{P^2T}$, where **P** is the beam polarization, and **T** is the beam transmission. An ideal polarizer will have **P** = 1 and **T** = 0.5, leading to a maximum possible metric value of $\mathbf{P^2T}$ = 0.5. In practice, $\mathbf{P^2T}$ of 0.30-0.35 is considered high values. Fe/Si polarizing supermirrors with high reflectivity up to m = 5.5 are commercially available. In our cases, Fe/Si polarizing supermirrors with m > 3 is necessary to provide high polarization for thermal neutrons with λ_{min} <= 1.5 Å. However, it requires a shallow incident angle (V_{angle} = 0.6°, i.e., the taper angle of the mirror surface and the beam axis = 0.3°) to use m = 3 mirrors, which will lead to a very low T for long-wavelength neutrons and reduce the useful wavelength bands. This can be overcome using high-m coating mirrors, as Figure 2-16 shows two designs with m = 4 and m = 5 double-side coated (Fe/Si) mirrors, respectively.

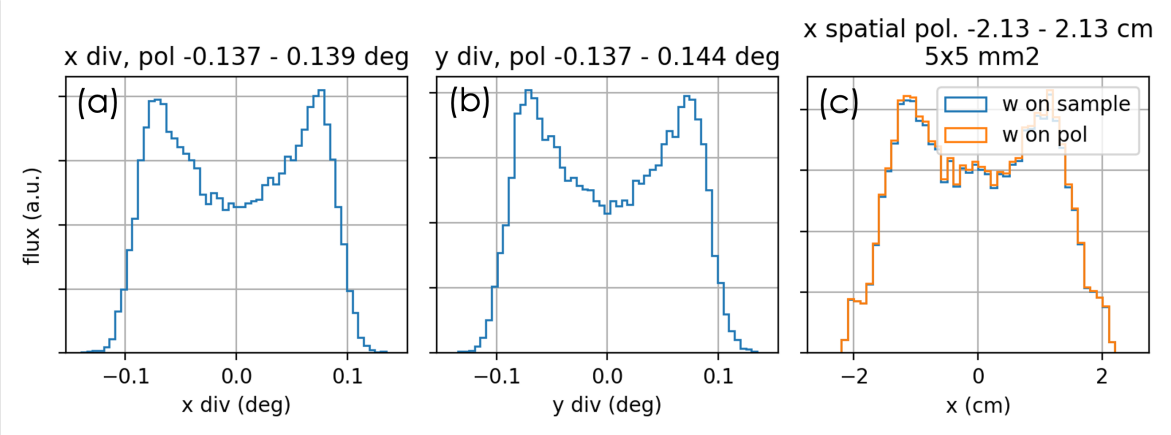

Figure 2-15 Simulated effective beam profiles (unpolarized beam) at the entrance of the polarization V-cavity. Only neutrons arrive within a 5×5 mm^2 central at the sample location are considered. (a), (b) the effective horizonal and vertical divergence profiles and (c) the effective spatial profiles using the neutron weights at the sample position and at the entrance of the polarizer. The small difference between the two curves in (c) is a signature of the high neutron transportation efficiency of the optimized neuron guide.

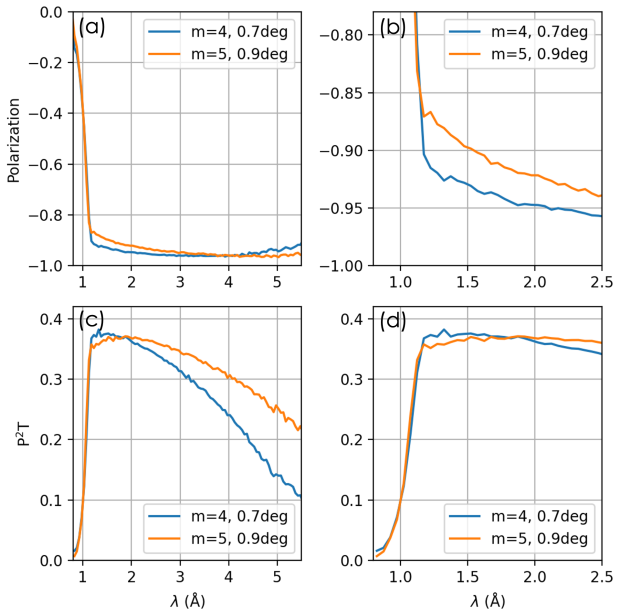

Figure 2-16 Simulated performance of two multichannel (n=3) polarizing V cavities with the shortest cutoff wavelength λ_{cutoff} = 1.2 Å. (a) and (b) are the polarization over a wide and a narrow wavelength ranges, respectively. (c) and (d) are the metric P^2T over a wide and a narrow wavelength range, respectively.

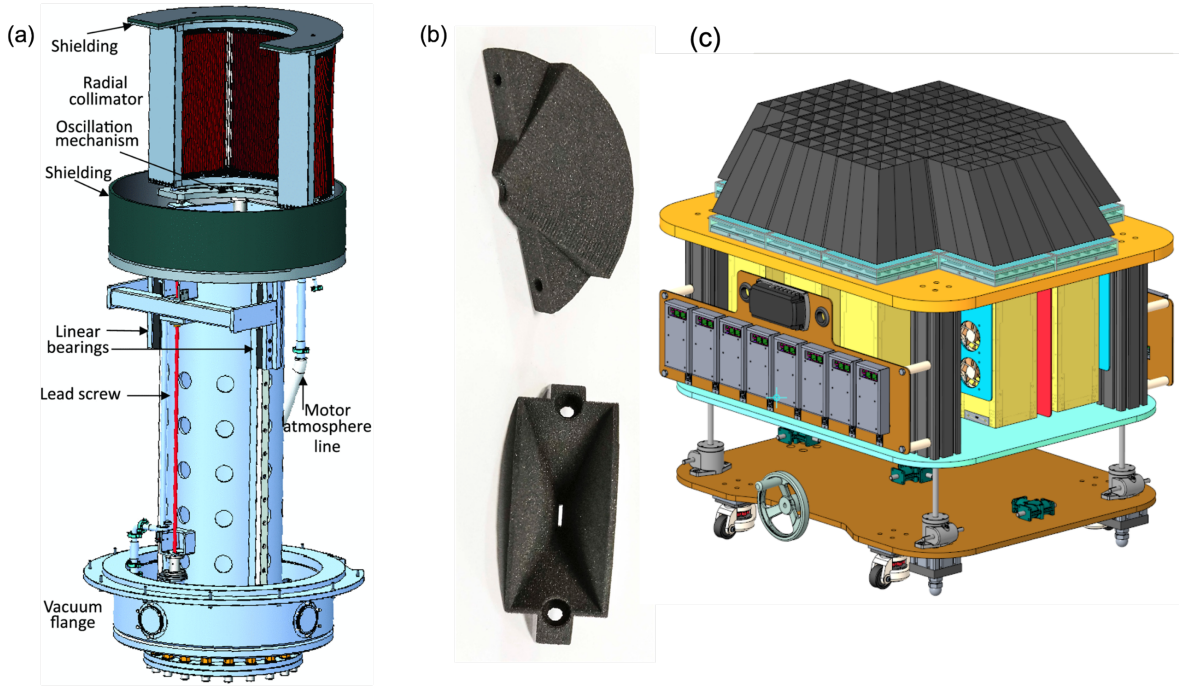

Figure 2-17 (a) The radial collimator designed for ARCS, SNS, (b) Examples of small, 3D, printed B_4C neutron collimators. (c)The proposed roll-in bottom detector array with a 3D printed cone-collimator for PIONEER.

The simulations use 3-channel polarizing V cavities designed with the shortest cutoff wavelength λ_{cutoff} = 1.2 Å, which requires V_{angle} = 0.7° (0.9°) and the mirror length of 1.22 m (0.95 m) with m = 4 (m = 5) mirrors. R_0=0.99 was assumed during simulations to count for imperfection, which limits the maximum possible polarization of 99%. Beam attenuation effects due to the FeSi deposited layer and Si wafter are considered based on the incoherent scattering and absorption cross-sections. The refraction effects are ignored because of their minor effect on the beam attenuation (O(1e-3)). The inner surfaces of the cavity will be coated with absorptive materials (m=0). Dividing walls are not used in the models because our simulations do not show performance improvement with absorptive dividing walls. Figure 2-16(a) and (b) compare the polarization levels between the two cases. The average polarization levels are similar for the 1.2-5.5 Å neutrons, but the m = 5 cavity leads to a relatively lower polarization for 1.5-Å neutrons than the m = 4 one. This is caused by the lower reflectivity below the critical edge for high-m mirrors (see Appendix B for details).

Figure 2-16(c) and (d) shows the $\mathbf{P^2T}$ values for the two cases. The $\mathbf{P^2T}$ values are comparable below 2.5 Å between the two cases. However, the m = 5 cavity shows much higher $\mathbf{P^2T}$ for longer wavelength neutrons. This is because using m = 5 mirrors allows a higher V_{angle} for a fixed shortest cutoff wavelength, leading to higher transmission for long-wavelength neutrons. Therefore, a 3-channel polarizing V cavity with m = 5 and V_{angle} = 0.9° will better match PIONEER's science needs.

2.3.7 Scattering beam collimators

The vertical cylindrical detector will work with an oscillating radial collimator (ORC). We plan to use a similar design to the one used at ARCS [19] and multiple other beamlines, including CORELLI and POWGEN. For the bottom flat detector, we plan to design a 3D-printed conical collimator [20, 21]. Figure 2-17 shows the ARCS collimator, the 3D-printed B_4C collimator made at ORNL, and the proposed bottom detector array with a 3D-printed collimator.

The OSC will be installed between the vacuum thimble and the cylindrical detector, whose blades will have an inner and outer radius of R_1 = 525 and R_2 = 775 mm, respectively. We chose the blade separation of α = 0.8° to give rise to the maximum impact length $b \approx \frac{\alpha R_1 R_2}{R_2 - R_1} = 27.7$ mm [22]. The ORC will effectively

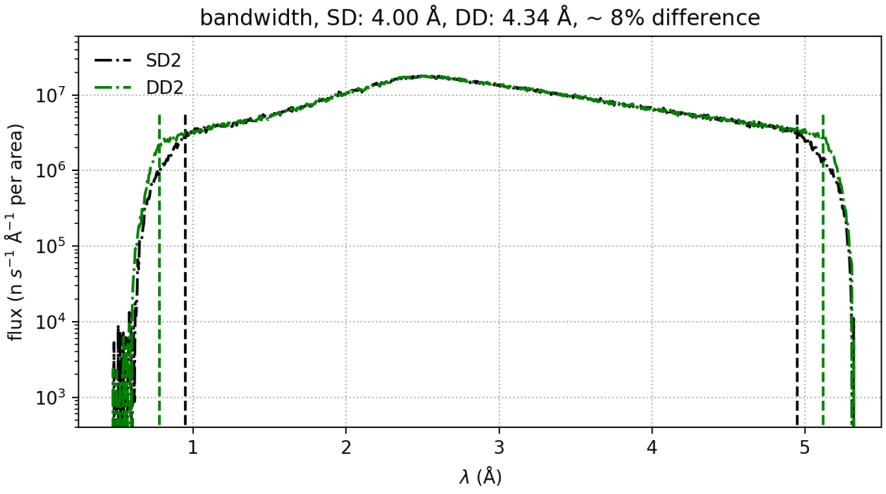

Figure 2-18 The effective bandwidth increases from 4.00 Å to 4.34 Å when the bandwidth definition chopper (the second disk chopper) changes from a single-disk large chopper to a double-disk large disk chopper.

reduce scattering events generated at locations with distances from the nominal sample beam larger than *b*. Therefore, the background scattering from large sample environments, such as a cryostat or a cryomagnet, will be significantly attenuated before reaching the detector. The OSC shall use the shift-mode operation mode to reduce the shadow effect [23].

2.4 NEUTRON CHOPPERS (WBS S.04.05.03)

PIONEER will use two standard large STS disk choppers for bandwidth control. The two choppers will be mounted inside the bunker to reduce the shielding requirement. The first is a frame-overlap chopper to block colder neutrons from the previous pulse, and the second is a wavelength-band definition chopper. The locations of the two choppers are very flexible, but the relative locations of the two choppers are important to avoid leakage.

We have chosen a single-disk (SD) STS chopper as the frame-overlap chopper and a double-disk (DD) STS chopper as the wavelength-band definition chopper. The double-disk chopper will lead to sharper rising edges, increasing the effective bandwidth for experiments. Figure 2-18 compares the simulated spectra using a single-disk chopper and a double-disk chopper as the wavelength-band definition chopper. In both cases, the frame-overlap chopper is an SD chopper. It shows that using a DD chopper as the wavelength-band definition chopper will increase the wavelength band by 8%, which is particularly preferred for time-resolved studies.

2.5 SHIELDING (WBS S.04.05.04)

PIONEER operates with an intense beam. The shielding is both for the safety requirements and for reducing the scattering background. The instrument shielding spans from the bunker wall to the instrument cave. There is a beam stop after the instrument cave. Shielding optimization is essential and must consider both the cost and the efficiency. Potential hotspots include the T_0 chopper, the shutter, the slit packages, the polarizing V-cavity, and the beamstop.

2.6 DETECTOR AND BEAM MONITOR SYSTEMS (WBS S.04.05.05)

2.6.1 Scattering beam detectors

Figure 2-19 shows PIONEER's detector system, which contains a large vertical cylindrical array and a small bottom flat array. Traditional TOF single-crystal diffractometers use a spherical detector system, such as TOPAZ or MaNDi at FTS. PIONEER will support multiple complex sample environments. When studying small samples or weak signals, it is necessary to use the scattering beam collimator to remove the secondary scattering from the sample environment. The spherical geometry makes it challenging to use an oscillating scattering-beam collimator. A feasible technical solution for the spherical detector geometry has yet to be identified. Therefore, we use a vertical cylindrical detector array compatible with an oscillating scattering-beam collimator. We plan to use neutron Anger cameras based on the magnetic-field-insensitive silicon photomultiplier (SiPM) [24] with a pixel pitch of 7.2 mm and a spatial resolution of 0.6 mm or better. The vertical and bottom arrays have 159 and 16 cameras, respectively. Each camera has a flat area of 174 ×174 mm^2, consisting of 3 × 3 SiPM units. One camera is removed along the incident beam direction to leave space for the get-lost tube.

We have designed a support structure to minimize the neutron-insensitive region between cameras, and in the current design, this is about 8-mm, which is about a pixel pitch. The straight beam will be offset from the center of the open space to render an asymmetric camera arrangement to minimize the potential impact from the dead regions between adjacent cameras. The cylindrical detector has a sample-to-detector distance of 0.8 m, accommodating various sample environments (SEs) for materials science with the collimator in

place. The vertical cylindrical array covers a 4.2 sr solid angle, with a 260° horizontal and 80° vertical range, and the bottom detector array coverage is 0.4 sr.

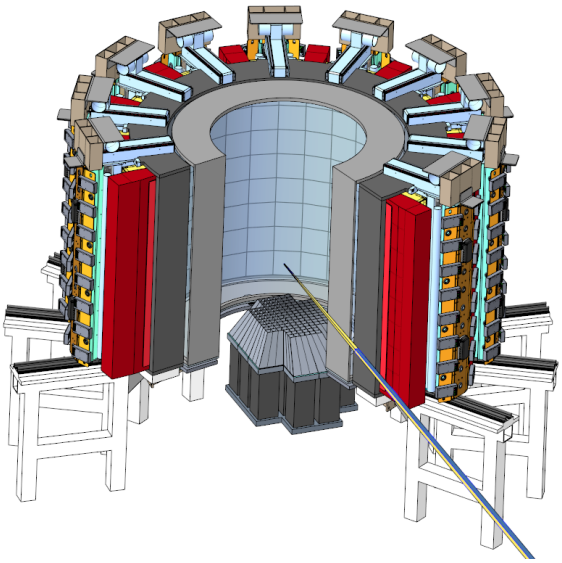

Figure 2-19 The PIONEER detector system contains a vertical cylindrical array with an oscillating radial collimator and a removable bottom flat array with a cone collimator. The radial collimator is omitted for clarity. The last portion of the neutron flight tube is included to indicate the direct beam direction.

We will calibrate the detector system during operation, including position and efficiency. However, we need to keep the detector efficiency stable during operation. PIONEER's large cylindrical detector array will generate a significant heat load during operation due to the many cameras involved. PIONEER will have 175 SiPM Anger cameras installed in proximity, each producing an estimated 65 W of heat. The total heat dissipation for the upper cylindrical array with 159 cameras is roughly 10.3 kW. As mentioned earlier, the cameras are arranged to optimize detector coverage to preclude using a traditional ambient air fan cooling solution. Therefore, to maintain acceptable temperature stability of ±1.5°C to ensure a nearly constant detector efficiency, an air-conditioned cooling system has been conceptualized for the PIONEERs detector system. The cooling system will consist of a heat exchanger, duct work, and fans to move cooled air across each camera.

The position calibration procedure highly depends on the initial input parameters; therefore, we need a position precision and repeatability for each camera to be better or comparable to the resolution, i.e., about 600 μm in the detector surface plane (from the scattering angle uncertainty), and along the *r* direction (from the time-of-flight uncertainty) to minimize the potential difficulty associated with changing the detector positions or the detector maintenance.

2.6.2 Incident beam monitors

Here we will discuss the requirement for the beam monitors used at PIONEER, which are primarily for diagnostic purposes and shall be translatable to be moved during regular operation. The only exception is the last monitor inside the get-lost-tube, which will be fixed. The details of the monitor positions can also be found in Table 2-2.

2.7 MOTION SYSTEMS (WBS S.04.05.06)

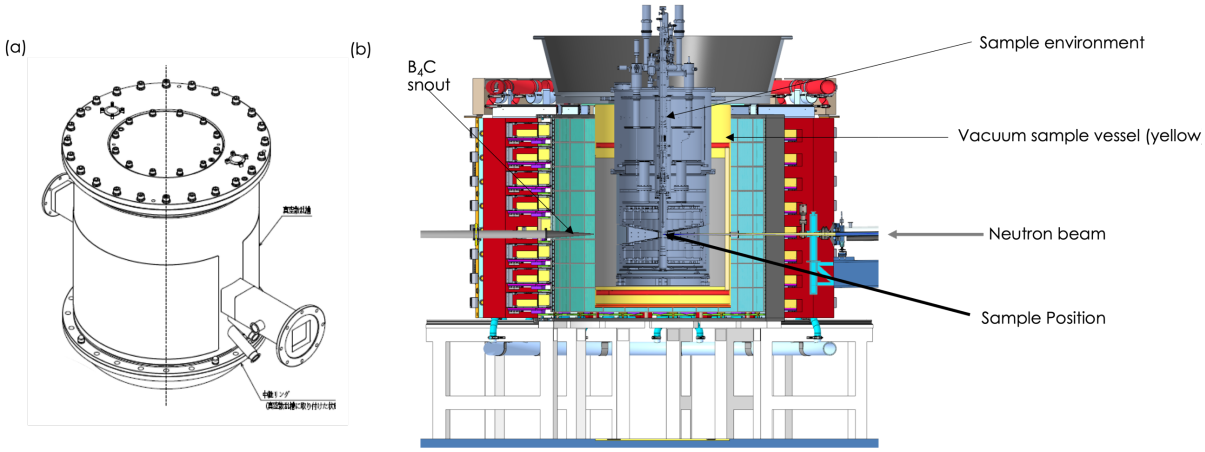

Figure 2-20 (a) The vacuum sample vessel used at SENJU. (Courtesy from Takashi OHHARA @ J-PARC) (b) The section view at the end station shows a medium sample environment (a 14-T superconducting magnet) inside the vacuum sample vessel. The radial oscillating collimator is omitted for clarity.

The motion systems at PIONEER include the maintenance shield and the shutter, and a translation table for the V-cavity polarizer, an elevator (3000 lb.) system for sample environment changes, an oscillating radial collimator (see section 2.3.7), and a removable bottom detector, and an auto-sample changer with a six-axis robotic arm.

2.7.1 Auto-sample changer with cryostream

We plan to use a six-axis robotic sample changer to enable highly automated experiments at PIONEER, similar to what has been done in multiple macromolecular X-ray crystallography beamlines [25]. The bottom detector array will be removed to enable this mode, and a high-precision goniometer will roll in. A cryostream like what is used at TOPAZ is planned to provide the temperature control on the sample over 90 K to 450 K.

2.8 INSTRUMENT SPECIFIC SYSTEMS (WBS S.04.05.07)

2.8.1 Vacuum sample vessel

A vacuum sample vessel is under consideration to reduce air scattering and work with multiple sample environments. Figure 2-20(a) shows the drawing of the vacuum sample vessel used at SENJU, and a similar concept will be applied at PIONEER. Additional noses on the vacuum vessel provide an extended vacuum path for the direct beam. There are areas with thin windows to reduce the secondary scattering of the scattered beam from the vessel. This thin window's size will match the cylindrical detector's angular coverage. Figure 2-20(b) shows a section view near the end station at PIONEER, showing a 14-T magnet inside the vacuum sample vessel. The vessel's thin window is displayed in gray, and its thick supporting structure is shown in yellow and red.

2.8.2 Sample alignment

The smallest beam size will be 1.0 mm for typical experiments. In some extreme cases, beam size may be further reduced, e.g., experiments using an X-Ray DAC. To achieve high-quality data, the sample should

stay within a sphere of confusion of ± 50 μm after sample rotation. The centroid of the neutron beam at the sample position should be determined with a precision better than 50 μm, and we shall orient the sample rotation axis at an arbitrary angle to the neutron beam in the horizontal plane with an accuracy better than 0.04°, matching the detector angular resolution. The latter can be calculated from the ratio between the detector's spatial resolution and the sample-to-detector distance, 0.6 mm / 800 mm = 0.75 μrad ~ 0.04°.

2.9 SAMPLE ENVIRONMENTS (WBS S.04.05.08)

Table 2-6 Sample environments for PIONEER

Parameter	Value	Comments
Temperature		
standard	1.5K – 500K	close-cycled cryostat
ultralow T inserts	0.05-300 K	^{3}He Insert, T_{base} = 240mK Dilution Refrigeration Insert, T_{base} = 50 mK
furnace	300 K – 1700 K	
Magnetic field		
static field, max	Cryo-Magnet, 8T	0.05-300K, vertical, minimal requirement
	Cryo-Magnet, 14T	0.05-300K, vertical, preferred
pulse-field, max		1.5-300 K, horizontal best available at SNS
High Pressure		
clamp cell, max.	2 GPa	0.3 - 300 K
DAC, max.	> 45 GPa	0.3 - 300 K
Automation		
A goniometer stage and a robotic sample changer to accommodate automated experiments.		A cryo-stream system, 90 and 450 K.

The sample environments are listed in Table 2-6. The workhorse equipment will be a thin-tail cryostat and a cryomagnet compatible with ^{3}He and dilution inserts.

2.9.1 Low/high temperatures

PIONEER will have a dedicated thin-tail close-cycled cryostat (CCR) to provide a temperature range between 1.5 K to 500 K. When the CCR is in use, the rotation axis should support a continuous rotation with precision ± 0.01° within a range of 720°, and a step size no more than 0.01°. The end station will accept shared cryogenic equipment from the sample environment group. All generic liquid ^{4}He cryostats, ^{3}He inserts, dilution fridge inserts, and furnaces will be occasionally used. Temperatures in the 50 mK - 1700K range without a magnetic field shall be available for user experiments.

2.9.2 Static magnetic field, vertical

PIONEER needs a split-coil asymmetric cryomagnet system to provide >= 7 T (preferred 14 T) vertical fields with a temperature range between 1.5 K to 300 K without ultralow temperature inserts. The cryogenic insert of the magnet will be equipped with a two-axis goniometer. It should be compatible with ultralow temperature inserts to access the ultralow temperature region down to 50 mK. This cryomagnet shall

provide a minimum scattering window of ±15° vertically and 180° horizontally and incorporate an incident beam collimator section in its body.

2.9.3 High pressure

PIONEER shall support at least two pressure cell types, the CuBe cells and the diamond anvil cells (DACs). PIONEER provides a tunable beam size that matches the sample size and reduces the cell's background scattering.

2.9.4 Additional sample environments

Other sample environments required by PIONEER's science case includes pulsed magnetic fields and commercially available X-ray DACs, and uniaxial strain apparatus.

2.10 INFRASTRUCTURE & UTILITIES (BWS S.04.04.09)

The essential infrastructures for PIONEER's operation include sample preparation and storage, vacuum systems, compressed gas systems, cryogen systems, fire protection systems, and electric power systems.

2.10.1 Sample preparation and storage

We will provide one sample mounting station with an optical microscope. Additionally, we will need a dry N_2 desiccator for temporary sample storage at the beamline.

2.10.2 Vacuum systems

The shared vacuum system in the bunker serves the guide system (~ 5×10^{-3} torr). Three emergency dry pumps will be attached to the guide system in case of a sudden loss of vacuum in the bunker system. Standard STS dry pump systems will provide a vacuum for the two bandwidth choppers (10^{-5} torr). The sample scattering chamber will have its vacuum system providing a ~5×10^{-3} torr vacuum. Exhaust from the vacuum pumps will be vented to the atmosphere via HEPA filters. The SNS sample environment group will provide pumps and vacuum leak test systems for ultra-low temperature inserts (^{3}He insert and dilution refrigerator).

2.10.3 Compressed gas

PIONEER requires compressed air in conjunction with the sample environment to dry sample sticks. PIONEER requires dry N_2 gas to dry and clean samples and for temporary sample storage and compressed He gas to backfill cold sample chambers for sample changes. The dry N2 gas will be obtained from the STS Target Building utility. PIONEER will have a designated area to store N_2 and ^{4}He gas cylinders.

2.10.4 Cryogens

PIONEER requires liquid N_2 and liquid ^{4}He to cool down samples in conjunction with different sample environments. PIONEER will have a designated area to temporarily store Dewars (at least for a 120L liquid Nitrogen N_2 and a 200L He Dewar) at the beamline.

2.10.5 Fire Protection

An evaluation will identify the specific needs by the Fire Protection Engineer.

2.10.6 Power and HVAC

PIONEER will need standard electrical panels for the sample environment (including motion panels) and polarization coils. We will make provisions to increase the size of a few panels to 100 A to avoid overload when Cryo-magnets are attached. Instrument loads will be evaluated with our electrical engineers and specified in the final design phase.

2.11 INSTRUMENT CONTROLS AND DAQ (WBS S.06.04.05) AND PERSONNEL PROTECTION SYSTEMS (WBS S.06.06)

Instrument controls and DAQ, and personnel protection systems shall meet the requirements in **ORNL/S06040200-SR0001**, *Integrated Control Systems - Instruments Control and Data Acquisition Requirements Document*. ICS will provide the following systems:

- DAQ.
- Network.
- Racks.
- Wiring.
- Timing System.
- STS standard Personnel Protection System and Oxygen Deficiency Hazard equipment.

A related topic is the instrument system hazard. As stated in **STS-S01030000-ES0002, R00**, *Second Target Station Preliminary Hazard Analysis Report*, instrument systems hazards are identified during the SNS operation [26] are expected to also apply to the STS instruments. The identified categories include (i) chemical hazards, (ii) cryogenic hazards, (3) electrical hazards, (4) fire hazards, (5) magnetic field hazards, (6) mechanical hazards, (7) oxygen deficiency hazards, (8) radiation hazards, (9) vacuum and pressure hazards and (10) other hazards. A preliminary evaluation with the ESH team shows that all these hazards apply to the PIONEER system and shall be reviewed for safety as designs develop during preliminary and final design following SNS procedures. Features for accident mitigation and any credited engineered controls (CECs) will be added as required. Before an instrument begins operating, the Instrument Readiness Review (IRR) Committee will conduct a comprehensive safety review.

2.12 SCIENTIFIC SOFTWARE (WBS S.04.02)

The Scientific Software shall include programs and procedures to operate safely and efficiently within the context of the user program.

APPENDIX A. DIFFERENT NEUTRON GUIDE OPTIONS

We have studied four types of guide systems, including Montel mirrors (Montel, as known as nested Kirkpatrick-Baez or KB mirrors), curved guides (Bender), straight guides (Straight), and kinked guides (Kink). In this study, $L_{source\text{-}sample}$ = 60.0 m, the value in the original instrument proposal. A uniform supermirror coating with m = 6 was applied to benchmark the performance. In this study, we focused on the high-flux (HF) mode, where the phase-space region of interest is a 5x5 mm^2 square with a beam divergence of ±0.3° along the horizontal and vertical directions, representing the largest phase space required for PIONEER's scientific case.

Specifically, our optimization was aimed at three main goals: (1) high flux within the region of interest (ROI) to improve the signal, (2) low flux outside the ROI to reduce background noise, and (3) uniform beam to reduce systematic errors. The numerical optimization and data analysis software packages include McStas [11, 12], MCVine [13, 14], SciPy [15], and JupyterLab [16]. Gravity effects and non-total reflectivity below the critical momentum transfer have been considered during our simulations. The mirror coating requirements were analyzed after the geometric optimization. This appendix will describe different guide options and compare their performance. We will start with the ideal guide geometry and later discuss the effects of engineering imperfection, including guide misalignment and mirror figure errors.

A.1 *Overview of characteristics of different neutron guide systems*

Figure A-1 shows the optimized guide geometry for the four different guide systems. The straight beamline requires a T_0 chopper to eliminate high-energy neutrons and gamma radiation. While the Montel, curved, and kink options naturally avoid a direct line-of-sight between the moderator and the sample.

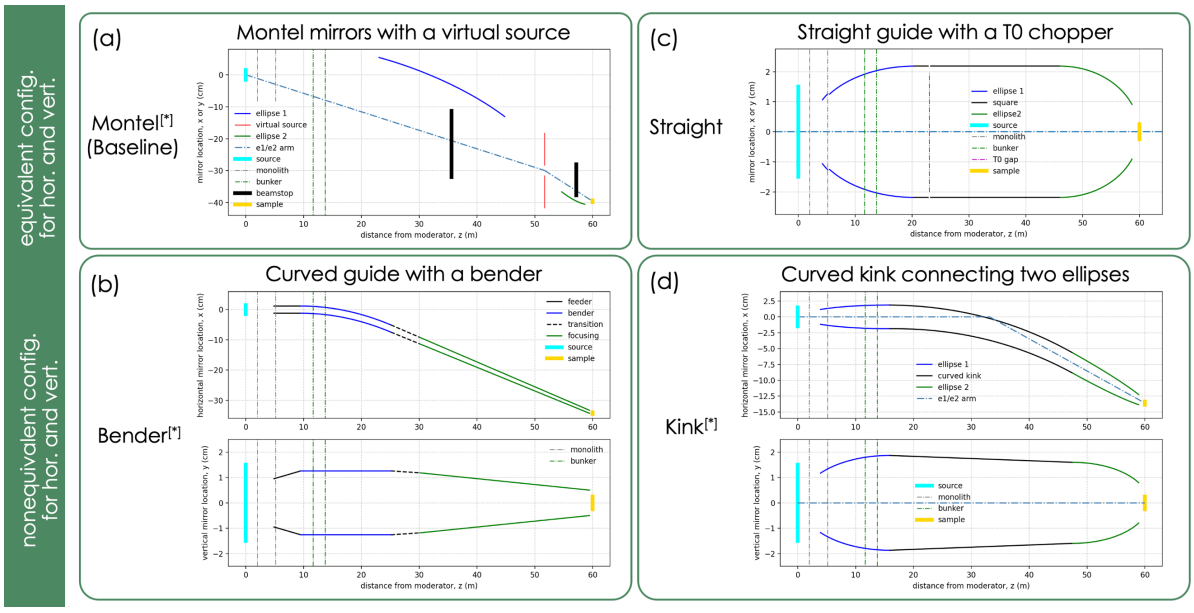

Figure A- 1 Schematic of four guide options after optimization for the high-flux mode. (a) Montel mirrors with a virtual source and built-in beamstop, (b) a curved beamline with a bender, (c) a straight beamline with a T0 chopper and two half-ellipse guides connected by a tapered section, and (d) a kinked beamline option with two half-ellipse guides connected by a curved section.

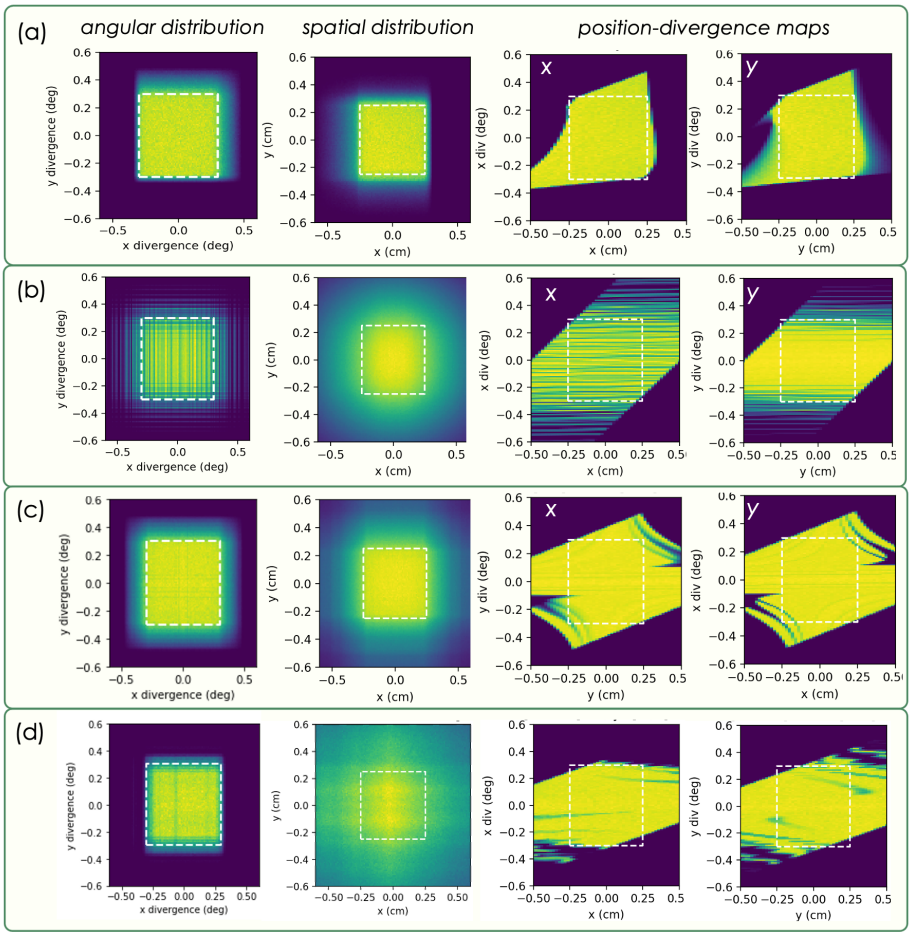

Figure A- 2 Two-dimensional slices in the four-dimensional phase space. From the left to right, the four columns are the spatial distributing, the angular distribution, and the position-divergence maps in the x and y directions, respectively. The four rows are results from the (a) Montel, (b) Bender, (c) Straight, and (d) Kink options, respectively. The white boxes are the chosen region of interest for the high-flux mode. The plots reflected the wavelength-integrated beam profiles over 1-5 Å.

Table A- 1 Flux comparison of the four guide options with ideal mirror geometries.

Flux with ROI (5 X 5 mm^2, ±0.3^o)	***Montel***	***Bender***	***Straight***	***Kink***
Flux at 1 Å [n s^{-1} cm^{-2} $^{-1}$Å^{-1}]	*2.5e7*	*5.5e7*	*9.6e7*	*8.6e7*
Peak Flux [n s^{-1} cm^{-2} Å^{-1}]	*3.1e8 at 2.6 Å*	*3.1e8 at 2.5 Å*	*4.2e8 at 2.5 Å*	*3.9e8 at 2.5 Å*
λ_{Cutoff} [Å], flux threshold	*1.35*	*< 0.8*	*< 0.8*	*< 0.8*
Effective Peak Flux [n s^{-1} cm^{-2} Å]	*2.4e9 at 3.3 Å*	*2.1e9 at 2.9 Å*	*2.9e9 at 2.9 Å*	*2.7e9 at 2.9 Å*
λ_{Cutoff} [Å], effective flux threshold	*1.35*	*1.20*	*0.95*	*1.00*
Integrated flux (1-5 Å) [n s^{-1} cm^{-2}]	*6.3e8*	*6.1e8*	*8.5e8*	*8.0e8*
Integrated flux (2-6 Å) [n s^{-1} cm^{-2}]	*6.1e8*	*5.6e8*	*7.6e8*	*7.2e8*
λ_{Cutoff} is determined using a flux threshold of 5e7 [n s^{-1} cm^{-2} Å^{-1}] or an effective flux threshold of 9e8 [n Å s^{-1} cm^{-2}].				

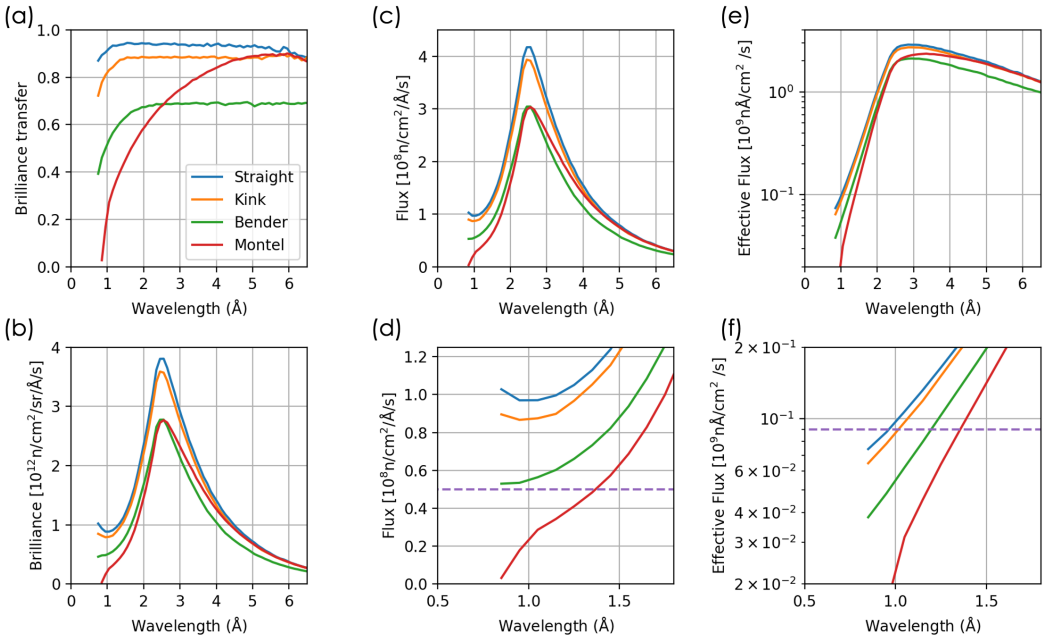

Figure A- 3 Brilliance and flux for the four guide options. (a) Brilliance transfer, and (b) brilliance, (c) flux and (e) effective flux at the sample position. (d) and (f) focus on the thermal neutron regions of (c) and (e).

Each option has advantages and disadvantages. Figure A-2 compares the spatial flux distribution and beam uniformity at the sample position. Figure A-3 shows the wavelength-dependent brilliance and the flux at the sample position. Brilliance transfer (BT) has been chosen as the metric to evaluate the neutron transport efficiency of different guides [27]. Table A-1 lists various flux values. Montel delivers fewer neutrons outside ROI at a high cost of thermal neutron flux. The Straight beamline delivers the brightest beam but delivers more neutrons outside the spatial ROI. Both the Bender and Kink options are less expensive, but their beam is less bright and less uniform, respectively, and both have even more neutrons outside the spatial ROI. The performance degradations are related to the bender [28] and the tapered regions [29]. All guide systems show a decrease in BT with decreasing wavelength at the short wavelength end, which is related to the reflectivity slope below the critical moment transfer of supermirrors. At the same time, the Montel mirrors show a strong wavelength dependence at the long wavelength end due to gravity effects, while the performances of the other three options are less sensitive to gravity.

This study has concluded that the straight beamline best matches PIONEER's science case. The straight beamline provides the brightest beam at the same position with abundant thermal neutrons at 1 Å and below. It delivers a uniform beam profile and shows good tolerance to various engineering imperfections. Below, we will describe each system in detail.

A.2 Montel mirrors

Figure A-1(a) presents the schematic drawing of the Montel mirror system. Each Montel mirror has two reflection surfaces and can accommodate a beam stop in the mirror region to block high-energy neutrons and gamma radiation without introducing a large gap. However, utilizing only two reflection surfaces results in a higher average reflection angle, which limits its ability to transport thermal neutrons with a sufficient beam divergence and necessitates a higher-m coating. The mirror geometry is symmetric between the horizontal and vertical directions. There is a lack of symmetry between the top and bottom directions and between the left and right directions, which results in the average beam direction being tilted away from the major axis of the Montel mirrors. Therefore, the major axes of the two Montel mirrors are intentionally tilted to achieve a truly horizontal beam at the sample position. We also introduced a kink between the two Montel mirrors to decrease the vertical

displacement of the beam, eliminating the need for a pit at the sample position. As shown in Figure A-3, the Montel system transports well for cold neutrons (> 2.0 Å) but not for thermal neutrons(< 1.5 Å).

Montel mirrors provide the most homogenous beam profiles, as shown in Figure A-2(a). The beam uniformity is related to the observation that all neutrons within the ROI are reflected once by each mirror surface (a total of four reflections) after the optimization. It also effectively controls the beam size at the sample position using the virtual source slit. However, the spatial and angular flux distributions are asymmetric, caused by the broken symmetry mentioned above and the aberration effect.

A.3 Curved beamline with a conventional bender

A beamline with a bender is a common design to avoid the direct line of sight. Figure A-1(b) presents the schematic drawing of a beamline with a single-channel bender, which performs slightly better than the multichannel option (n=3) regarding neutron transportation. Both options provide higher thermal-neutron flux than the Montel optics but lower flux for cold neutrons. This option yields the lowest wavelength integrated flux on the sample.

As seen from Figure A-2(b), there are high-frequency structures (period ~ 0.02-0.04º) in the angular distribution in the horizontal x-direction, which will not distort diffraction peak profiles or diffuse scattering patterns from real crystals but will reduce the flux within ROI. The phase space distortion from the bender causes inhomogeneity. The tapered guide after the bender provides two active roles: to focus the beam and to improve the phase-space homogeneity, achieved by an increased average number of bounces. As a result, there is a broad distribution of the number of bounces and reduced Brilliance transfer.

The curved beamline delivers a lower wavelength-integrated flux (1-5 Å) and a lower effective peak flux than the Montel optics, as shown in Table A-1. Additionally, there is no focusing point within the guide system to control the beam size effectively; therefore, a final beam aperture is necessary.

A.4 Straight beamline with two half-elliptical guides

Figure A-1(c) shows our straight beamline design, which uses two half-ellipse guides with a tapered section (approximated by multiple constant cross-section guides) in between. Recent studies show that elliptical guides perform superior neutron transport over long distances [30]. Compared to single-ellipse designs, our design reduces the maximum cross-section of the guide and provides a focal point (a virtual source) in the middle of the guide for beam size control. At the same time, the long-tapered section provides flexibility to introduce multiple large gaps (> 1 m) to install a T_0 chopper, a heavy shutter, and a polarizing V-cavity without significantly reducing the neutron transport performance.

The Straight option provides a higher thermal neutron flux and integrated flux than the Montel optics, while the peak fluxes are comparable. The beam profile is simpler and symmetric and is sufficiently homogeneous after optimization. However, it delivers more neutrons outside the ROI than the Montel option. The high-resolution mode can be achieved by replacing the second elliptical guide's last section (4-6 m) with a vacuum flight tube. We can also extend the second elliptical guide by a short focusing guide (~0.5 m) to further focus the beam for a higher flux on smaller samples.

A.5 Kinked beamline with two half-elliptical guides

The Kink design is modified from the straight beamline. As show in Figure A-1 (d), a kink is introduced between the major axes of the two half-ellipses to eliminate the T_0 chopper and heavy shutter. This option saves costs and has a comparable flux to the Straight option. However, it shows an increased phase-space inhomogeneity and more neutrons outside the spatial ROI. Further improvement on the beam profile homogeneity is required to use this option for SCND experiments on small crystals.

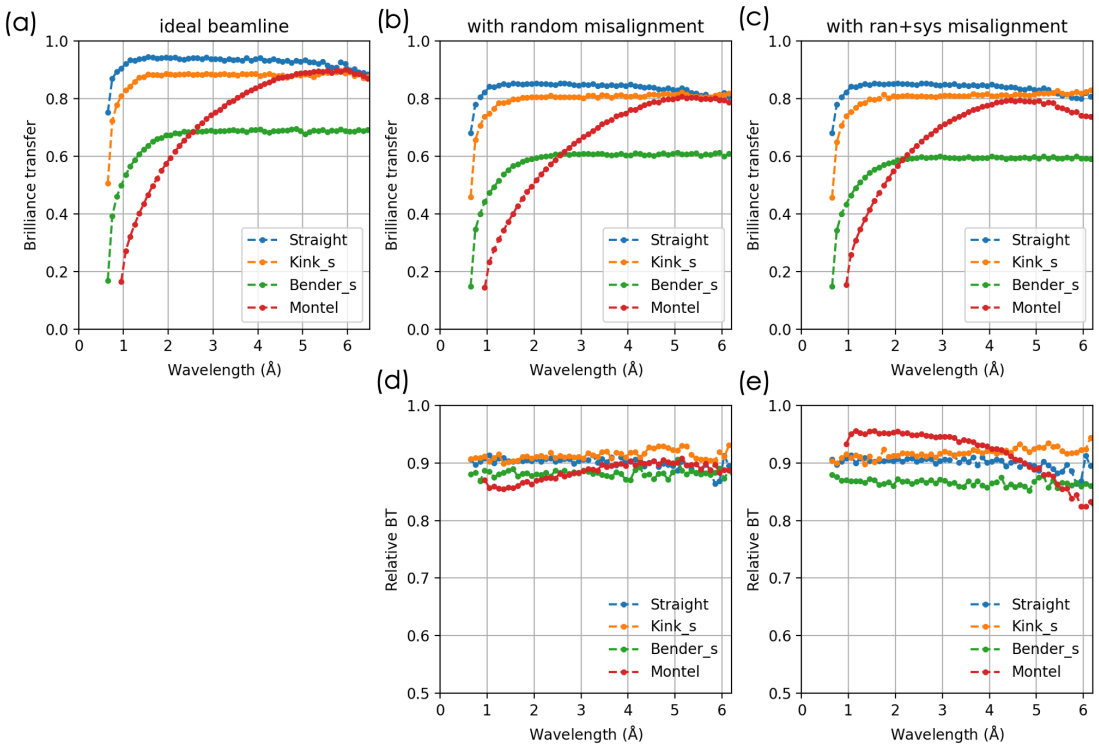

Figure A- 4 Misalignment effect on the brilliance transfer. (a) BTs for the four guides with idea geometries, (b) BTs with default random misalignment values, and (c) BTs with default random and systematic misalignment values. (d) and (e) relative BTs of the misalignment model with respect to the idea geometries.

A.6 Incident spectrum range

Neutrons of the shortest wavelength limit the accessible incident spectrum range. We have used a threshold value of the flux, or the effective flux, as a metric to determine the shortest wavelength for each option because it is a more relevant quantity than BTs for experiments. The effective flux for time-of-flight diffraction $\phi_{eff}(\lambda) = \phi(\lambda)\lambda^2$, where $\phi(\lambda)$ is the wavelength-dependent flux [31]. The results are summarized in Figure A-3 and Table A-1.

Using a flux threshold of $5\text{x}10^7$ [n s^{-1} cm^{-2} $Å^{-1}$], The Montel option shows a cutoff wavelength of 1.35 Å, corresponding to an effective flux of $9\text{x}10^8$ [n Å s^{-1} cm^{-2}]. All other options show a cutoff wavelength < 0.8 Å using the same flux threshold. However, based on the effective flux, the cutoff wavelengths are 1.20 Å, 0.95 Å, and 1.00 Å, for the Bender, the Straight, and the Kinked options.

A.7 Effects of guide misalignment

The misalignment effect was evaluated based on a previously published model [32]. Two types of misalignments are considered, random misalignment and systematic misalignment. The former is mainly from the mirror assembly with minor effects from the random vibration and thermal expansion. The latter is due to floor displacement with the maximum settlement locating near heavy structural loads, such as the bunker wall. The results are summarized in Figure A-4.

Figures A-4(b, d) show the changes in BTs from default random misalignment settings. The most influential quantity is the transverse element misalignment. The model uses an element length of 0.5 m and a transverse misalignment value of 20 µm. Figures A-4(c, e) shows the BT changes from a combined random and systematic misalignment with default values. The default value for the maximum floor displacement is 1.5 mm.

The Straight and Kink guides show similar sensitivity levels to the misalignments, and the Bender shows a slightly higher sensitivity. The similarity is unsurprising because these three guide systems have similar cross-

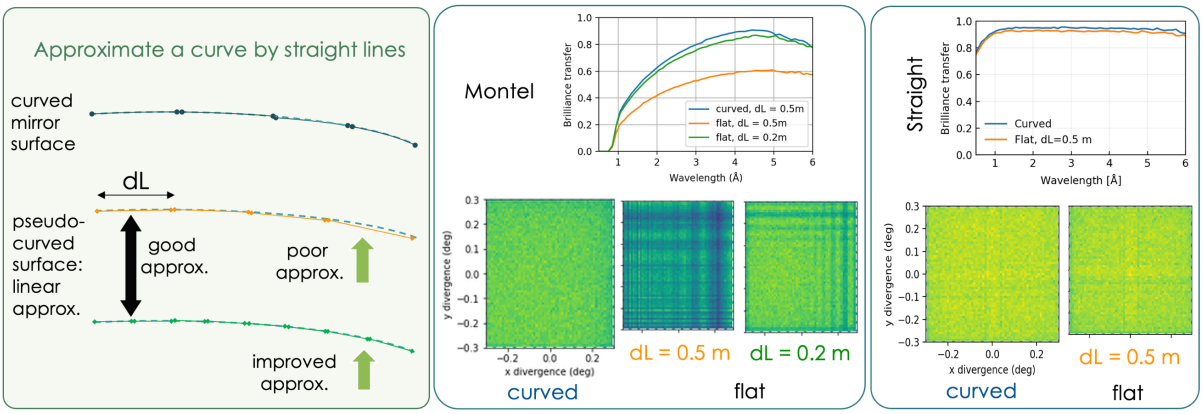

Figure A- 6 The effect of using flat substrates to approximate curved mirrors from models based on Montel mirrors and Straight beamlines.

sections and total guide lengths. The Montel option has a very different geometry, with two reflection surfaces per mirror with a kink between the two sets of Montel mirrors. Compared to the other three options, each reflection surfaces are much larger, and the total mirror length is shorter. The relative BT changes for the Montel option show a stronger wavelength dependence, which is also observed in the wavelength-dependent BTs mentioned previously.

Overall, the guide systems are most sensitive to the element transverse misalignment and not sensitive to a small gap between elements. To keep the relative flux loss less than 10%, the transverse element misalignment should be less than 20 µm. With the default random-misalignment values, BT shows little changes when the maximum floor displacement is less than 1.5 mm but shows enhanced sensitivity to the floor displacement when the maximum displacement exceeds 3 mm.

A.8 ***Effects of mirror figure errors***

We use the traditional evaluation method to describe the surface figure error, the root mean square (RMS). It is called mirror gaussian waviness in the McStas package [33]. The results for the Montel and Straight options are shown in Fig. 6. The waviness tolerance given by SwissNeutronics is < 1.5×10^{-4} rad. and the reported waviness values are better, 0.6-1.0 x 10^{-4} rad. We have evaluated how the wavelength-integrated BT changes as a function of the mirror waviness. Here we consider the two more relevant cases, the Montel and Straight options, and the results are shown in Figure A-5. Using the average value of 0.8 x 10^{-4} rad., the waviness will lead to a 5% reduction in BT for the Montel option and 1.5% reduction for the Straight beamline.

The geometric form of mirror substrates is related to figure error. All four options contain sections with curved mirrors. However, low figure-error curved substrates are costive. At beamlines, an array of tapered mirror/guide elements is often used to approximate long curved/elliptical mirrors. As shown in Figure A-6, shorter flat elements lead to a better curve approximation. However, using shorter elements will reduce the performance due to mirror misalignment. On the other hand, the typical lengths of individual mirrors provided by vendors are 0.5-m or less.

For the Montel option, the beam profile will be distorted with the BT is significantly reduced when 0.5-m mirror elements are used for the whole beamline. To approximate the Montel mirrors, individual element length, at least for the second mirror, must be shorter than 0.2 m. In contrast, 0.5-m flat substrates for the full Straight beamline show a minor reduction in performance.

APPENDIX B. ELEMENT-WISE M-COATING OPTIMIZATION

Real supermirrors reflect neutrons with a reflectivity less than the ideal value 1. Supermirrors with *m*-value up to 8 are commercially available. The reflectivity drops rapidly at a supermirror's extended critical scattering vector, $q_c = m \times q^{Ni}$, where $q^{Ni} = 0.0219$ Å^{-1} is the critical scattering wavevector for natural Ni. A linear function is typically used to approximate the reflection probability in the intermediate q values, i.e., $R(q) = R_0 (1 - \alpha(q - q^{Ni}))$ for $qc > q > q^{Ni}$, where R_0 is the reflective value below q^{Ni}.

As shown in Figure B-1, high-*m*-value supermirrors usually show a large slope on the reflectivity below its critical moment transfer value, i.e., high-*m*-value supermirrors may have a lower reflectivity at the lower wavevector transfer region than low-*m*-value supermirrors. Therefore, choosing the m-value sufficient for the science need will save cost and help improve the performance.

The workflow used to optimize the required *m*-profile has been introduced in Section 2.3.3. In practice, we determine multiple *m*-profiles by varying the requirement of the cut-off wavelength λ_{cutoff}, the preferred beam size, and divergence. And we compare the simulated results using these m-profiles. Figure B-2 shows an example. We have generated three m profiles based on different criteria: low, intermediate, and high-m. The simulated fluxes based on the three profiles are shown at the bottom. The same α value was used for the three simulations, therefore, the wavelength dependent fluxes are same at the long wavelength limit, but shows different values at the short-wavelength limit. It shows that the intermediate-*m* profile is sufficient to transport 1- Å neutrons for PIONEER's science case. This option will cost less than the high-m or uniform-m coating profile.

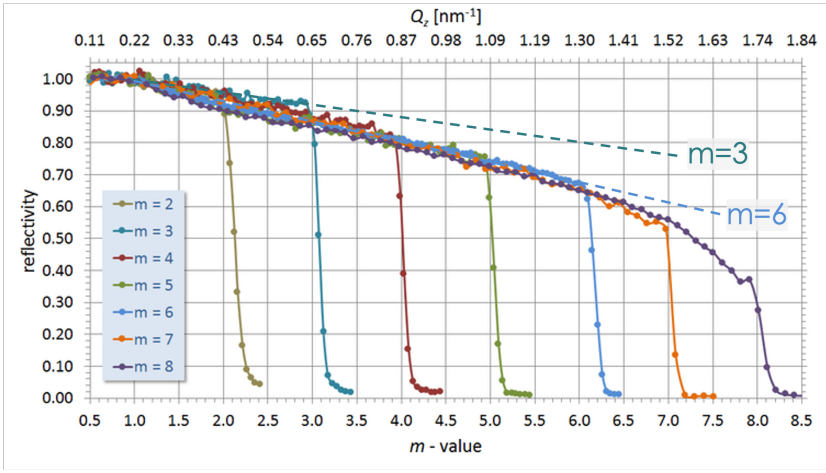

Figure B- 1 Reflectivity of state-of-the-art supermirrors with different m-value coating (adapted from https://www.swissneutronics.ch/products/neutron-supermirrors/). It shows that high m-value mirrors show higher slopes under the critical edge, giving less ideal total reflection at the low wavevector transfer region.

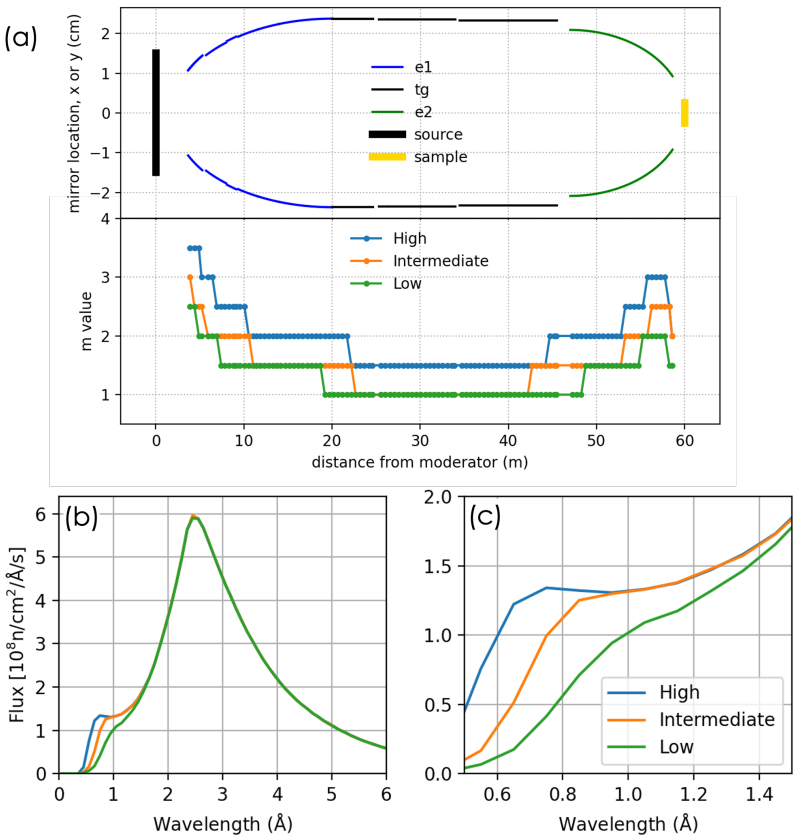

Figure B- 2 (a) three m-profiles generated from different criteria. (b) and (c) the wavelength dependent flux based on the three m-profiles.

APPENDIX C. INSTRUMENT MCSTAS FILE

```
#
# VERSION: ETE_V033
# liuyh@ornl.gov, June 06, 2023
#
DEFINE INSTRUMENT myinstrument()
DECLARE
%{

%}
INITIALIZE
%{

%}
TRACE
COMPONENT origin = Arm(

)
AT (0.0, 0.0, 0) ABSOLUTE
ROTATED (0.0, 0.0, 0.0) ABSOLUTE

COMPONENT e1_arm = Arm(

)
AT (0.0, 0.0, 0) ABSOLUTE
ROTATED (0.0, 0.0, 0.0) ABSOLUTE

COMPONENT e11_arm = Arm(

)
AT (0.0, 0.0, 2.5883) ABSOLUTE
ROTATED (0.0, 0.0, 0.0) ABSOLUTE

COMPONENT main_shutter_arm = Arm(

)
AT (0.0, 0.0, 5.294) ABSOLUTE
ROTATED (0.0, 0.0, 0.0) ABSOLUTE

COMPONENT e12_arm = Arm(

)
AT (0.0, 0.0, 5.5842) ABSOLUTE
ROTATED (0.0, 0.0, 0.0) ABSOLUTE

COMPONENT SD_arm = Arm(

)
AT (0.0, 0.0, 7.776) ABSOLUTE
ROTATED (0.0, 0.0, 0.0) ABSOLUTE

COMPONENT e13_arm = Arm(

)
AT (0.0, 0.0, 7.819) ABSOLUTE
ROTATED (0.0, 0.0, 0.0) ABSOLUTE

COMPONENT DD_arm = Arm(

)
AT (0.0, 0.0, 9.382000000000001) ABSOLUTE
ROTATED (0.0, 0.0, 0.0) ABSOLUTE

COMPONENT e14_arm = Arm(

)
AT (0.0, 0.0, 9.592) ABSOLUTE
ROTATED (0.0, 0.0, 0.0) ABSOLUTE
```

```
COMPONENT e15_arm = Arm(

)
AT (0.0, 0.0, 11.528) ABSOLUTE
ROTATED (0.0, 0.0, 0.0) ABSOLUTE

COMPONENT e16_arm = Arm(

)
AT (0.0, 0.0, 13.926) ABSOLUTE
ROTATED (0.0, 0.0, 0.0) ABSOLUTE

COMPONENT tg1_arm = Arm(

)
AT (0.0, 0.0, 17.425500000000003) ABSOLUTE
ROTATED (0.0, 0.0, 0.0) ABSOLUTE

COMPONENT T0_arm = Arm(

)
AT (0.0, 0.0, 25.1) ABSOLUTE
ROTATED (0.0, 0.0, 0.0) ABSOLUTE

COMPONENT OP_shutter_arm = Arm(

)
AT (0.0, 0.0, 25.810000000000002) ABSOLUTE
ROTATED (0.0, 0.0, 0.0) ABSOLUTE

COMPONENT tg2_arm = Arm(

)
AT (0.0, 0.0, 26.834000000000003) ABSOLUTE
ROTATED (0.0, 0.0, 0.0) ABSOLUTE

COMPONENT vs_arm = Arm(

)
AT (0.0, 0.0, 34.0006) ABSOLUTE
ROTATED (0.0, 0.0, 0.0) ABSOLUTE

COMPONENT tg3_arm = Arm(

)
AT (0.0, 0.0, 34.5715) ABSOLUTE
ROTATED (0.0, 0.0, 0.0) ABSOLUTE

COMPONENT pol_arm = Arm(

)
AT (0.0, 0.0, 43.6715) ABSOLUTE
ROTATED (0.0, 0.0, 0.0) ABSOLUTE

COMPONENT e21_arm = Arm(

)
AT (0.0, 0.0, 45.4645) ABSOLUTE
ROTATED (0.0, 0.0, 0.0) ABSOLUTE

COMPONENT sample_arm = Arm(

)
AT (0.0, 0.0001, 56.0) ABSOLUTE
ROTATED (0.0, 0.0, 0.0) ABSOLUTE

COMPONENT moderator = STS_Source(
   Emin=2.0, Emax=120.0, dist=2.4, filename=" BL13-CY-46D-STS-Min-2G-source_mctal-125_sp.dat", focus_xw=0.024, focus_yh=0.024,
xwidth=0.03, yheight=0.03
```

```
)
AT (0, 0, 0) RELATIVE origin

COMPONENT E11_0 = Guide_gravity(
   l=0.2192336666666669, w1=0.023746418646804584, h1=0.023746418646804584, w2=0.025243770072470532,
h2=0.025243770072470532, mleft=3.5, mtop=3.5, mright=3.5, mbottom=3.5, alpha=3.044, G=-9.81, wavy=0.0057
)
AT (0.0, 0.0, 2.5883) RELATIVE e1_arm
ROTATED (0, 0, 0) RELATIVE e1_arm

COMPONENT E11_1 = Guide_gravity(
   l=0.4384673333333338, w1=0.025243770072470532, h1=0.025243770072470532, w2=0.027941002934162792,
h2=0.027941002934162792, mleft=3.5, mtop=3.5, mright=3.5, mbottom=3.5, alpha=3.044, G=-9.81, wavy=0.0057
)
AT (0.0, 0.0, 2.807533666666667) RELATIVE e1_arm
ROTATED (0, 0, 0) RELATIVE e1_arm

COMPONENT E11_2 = Guide_gravity(
   l=0.5, w1=0.027941002934162792, h1=0.027941002934162792, w2=0.03064277060190606, h2=0.03064277060190606, mleft=3.0,
mtop=3.0, mright=3.0, mbottom=3.0, alpha=3.044, G=-9.81, wavy=0.0057
)
AT (0.0, 0.0, 3.2460010000000006) RELATIVE e1_arm
ROTATED (0, 0, 0) RELATIVE e1_arm

COMPONENT E11_3 = Guide_gravity(
   l=0.5, w1=0.03064277060190606, h1=0.03064277060190606, w2=0.03303949186364401, h2=0.03303949186364401, mleft=3.0, mtop=3.0,
mright=3.0, mbottom=3.0, alpha=3.044, G=-9.81, wavy=0.0057
)
AT (0.0, 0.0, 3.7460010000000006) RELATIVE e1_arm
ROTATED (0, 0, 0) RELATIVE e1_arm

COMPONENT E11_4 = Guide_gravity(
   l=0.5, w1=0.03303949186364401, h1=0.03303949186364401, w2=0.03519354404300845, h2=0.03519354404300845, mleft=2.5, mtop=2.5,
mright=2.5, mbottom=2.5, alpha=3.044, G=-9.81, wavy=0.0057
)
AT (0.0, 0.0, 4.246001000000001) RELATIVE e1_arm
ROTATED (0, 0, 0) RELATIVE e1_arm

COMPONENT E11_5 = Guide_gravity(
   l=0.5, w1=0.03519354404300845, h1=0.03519354404300845, w2=0.0371471660999755, h2=0.0371471660999755, mleft=2.5, mtop=2.5,
mright=2.5, mbottom=2.5, alpha=3.044, G=-9.81, wavy=0.0057
)
AT (0.0, 0.0, 4.746001000000001) RELATIVE e1_arm
ROTATED (0, 0, 0) RELATIVE e1_arm

COMPONENT E12_0 = Guide_gravity(
   l=0.5, w1=0.036710252440117094, h1=0.036710252440117094, w2=0.03831881615284545, h2=0.03831881615284545, mleft=2.5,
mtop=2.5, mright=2.5, mbottom=2.5, alpha=3.044, G=-9.81, wavy=0.0057
)
AT (0.0, 0.0, 5.5842) RELATIVE e1_arm
ROTATED (0, 0, 0) RELATIVE e1_arm

COMPONENT E12_1 = Guide_gravity(
   l=0.5, w1=0.03831881615284545, h1=0.03831881615284545, w2=0.03979758874537049, h2=0.03979758874537049, mleft=2.5, mtop=2.5,
mright=2.5, mbottom=2.5, alpha=3.044, G=-9.81, wavy=0.0057
)
AT (0.0, 0.0, 6.0842) RELATIVE e1_arm
ROTATED (0, 0, 0) RELATIVE e1_arm

COMPONENT E12_2 = Guide_gravity(
   l=0.5, w1=0.03979758874537049, h1=0.03979758874537049, w2=0.04116056158493628, h2=0.04116056158493628, mleft=2.0, mtop=2.0,
mright=2.0, mbottom=2.0, alpha=3.044, G=-9.81, wavy=0.0057
)
AT (0.0, 0.0, 6.5842) RELATIVE e1_arm
ROTATED (0, 0, 0) RELATIVE e1_arm

COMPONENT E12_3 = Guide_gravity(
   l=0.5, w1=0.04116056158493628, h1=0.04116056158493628, w2=0.04241889851800312, h2=0.04241889851800312, mleft=2.0, mtop=2.0,
mright=2.0, mbottom=2.0, alpha=3.044, G=-9.81, wavy=0.0057
)
```

```
AT (0.0, 0.0, 7.0842) RELATIVE e1_arm
ROTATED (0, 0, 0) RELATIVE e1_arm

COMPONENT E13_0 = Guide_gravity(
   l=0.5, w1=0.04204186162531422, h1=0.04204186162531422, w2=0.043138040494123626, h2=0.043138040494123626, mleft=2.0,
mtop=2.0, mright=2.0, mbottom=2.0, alpha=3.044, G=-9.81, wavy=0.0057
)
AT (0.0, 0.0, 7.819) RELATIVE e1_arm
ROTATED (0, 0, 0) RELATIVE e1_arm

COMPONENT E13_1 = Guide_gravity(
   l=0.5, w1=0.043138040494123626, h1=0.043138040494123626, w2=0.044151022772201655, h2=0.044151022772201655, mleft=2.0,
mtop=2.0, mright=2.0, mbottom=2.0, alpha=3.044, G=-9.81, wavy=0.0057
)
AT (0.0, 0.0, 8.318999999999999) RELATIVE e1_arm
ROTATED (0, 0, 0) RELATIVE e1_arm

COMPONENT E13_2 = Guide_gravity(
   l=0.5, w1=0.044151022772201655, h1=0.044151022772201655, w2=0.045086416484330684, h2=0.045086416484330684, mleft=2.0,
mtop=2.0, mright=2.0, mbottom=2.0, alpha=3.044, G=-9.81, wavy=0.0057
)
AT (0.0, 0.0, 8.818999999999999) RELATIVE e1_arm
ROTATED (0, 0, 0) RELATIVE e1_arm

COMPONENT E14_0 = Guide_gravity(
   l=0.41500099999999907, w1=0.04458772143618867, h1=0.04458772143618867, w2=0.04526208057935405, h2=0.04526208057935405,
mleft=2.0, mtop=2.0, mright=2.0, mbottom=2.0, alpha=3.044, G=-9.81, wavy=0.0057
)
AT (0.0, 0.0, 9.592) RELATIVE e1_arm
ROTATED (0, 0, 0) RELATIVE e1_arm

COMPONENT E14_1 = Guide_gravity(
   l=0.5, w1=0.04526208057935405, h1=0.04526208057935405, w2=0.04601434617910775, h2=0.04601434617910775, mleft=2.0, mtop=2.0,
mright=2.0, mbottom=2.0, alpha=3.044, G=-9.81, wavy=0.0057
)
AT (0.0, 0.0, 10.007000999999999) RELATIVE e1_arm
ROTATED (0, 0, 0) RELATIVE e1_arm

COMPONENT E14_2 = Guide_gravity(
   l=0.5, w1=0.04601434617910775, h1=0.04601434617910775, w2=0.04670379356136105, h2=0.04670379356136105, mleft=2.0, mtop=2.0,
mright=2.0, mbottom=2.0, alpha=3.044, G=-9.81, wavy=0.0057
)
AT (0.0, 0.0, 10.507000999999999) RELATIVE e1_arm
ROTATED (0, 0, 0) RELATIVE e1_arm

COMPONENT E14_3 = Guide_gravity(
   l=0.5, w1=0.04670379356136105, h1=0.04670379356136105, w2=0.04733316780616236, h2=0.04733316780616236, mleft=2.0, mtop=2.0,
mright=2.0, mbottom=2.0, alpha=3.044, G=-9.81, wavy=0.0057
)
AT (0.0, 0.0, 11.007000999999999) RELATIVE e1_arm
ROTATED (0, 0, 0) RELATIVE e1_arm

COMPONENT E15_0 = Guide_gravity(
   l=0.38300099999999926, w1=0.04728897641403119, h1=0.04728897641403119, w2=0.04772946083836419, h2=0.04772946083836419,
mleft=2.0, mtop=2.0, mright=2.0, mbottom=2.0, alpha=3.044, G=-9.81, wavy=0.0057
)
AT (0.0, 0.0, 11.528) RELATIVE e1_arm
ROTATED (0, 0, 0) RELATIVE e1_arm

COMPONENT E15_1 = Guide_gravity(
   l=0.5, w1=0.04772946083836419, h1=0.04772946083836419, w2=0.048255239381301974, h2=0.048255239381301974, mleft=2.0,
mtop=2.0, mright=2.0, mbottom=2.0, alpha=3.044, G=-9.81, wavy=0.0057
)
AT (0.0, 0.0, 11.911000999999999) RELATIVE e1_arm
ROTATED (0, 0, 0) RELATIVE e1_arm

COMPONENT E15_2 = Guide_gravity(
   l=0.5, w1=0.048255239381301974, h1=0.048255239381301974, w2=0.04872688023183654, h2=0.04872688023183654, mleft=2.0,
mtop=2.0, mright=2.0, mbottom=2.0, alpha=3.044, G=-9.81, wavy=0.0057
)
```

```
AT (0.0, 0.0, 12.411000999999999) RELATIVE e1_arm
ROTATED (0, 0, 0) RELATIVE e1_arm

COMPONENT E15_3 = Guide_gravity(
   l=0.5, w1=0.04872688023183654, h1=0.04872688023183654, w2=0.04914594205083366, h2=0.04914594205083366, mleft=2.0, mtop=2.0,
mright=2.0, mbottom=2.0, alpha=3.044, G=-9.81, wavy=0.0057
)
AT (0.0, 0.0, 12.911000999999999) RELATIVE e1_arm
ROTATED (0, 0, 0) RELATIVE e1_arm

COMPONENT E15_4 = Guide_gravity(
   l=0.5, w1=0.04914594205083366, h1=0.04914594205083366, w2=0.049513759870921034, h2=0.049513759870921034, mleft=2.0,
mtop=2.0, mright=2.0, mbottom=2.0, alpha=3.044, G=-9.81, wavy=0.0057
)
AT (0.0, 0.0, 13.411000999999999) RELATIVE e1_arm
ROTATED (0, 0, 0) RELATIVE e1_arm

COMPONENT E16_0 = Guide_gravity(
   l=0.4995, w1=0.04947678949058641, h1=0.04947678949058641, w2=0.049792708931209094, h2=0.049792708931209094, mleft=2.0,
mtop=2.0, mright=2.0, mbottom=2.0, alpha=3.044, G=-9.81, wavy=0.0057
)
AT (0.0, 0.0, 13.926) RELATIVE e1_arm
ROTATED (0, 0, 0) RELATIVE e1_arm

COMPONENT E16_1 = Guide_gravity(
   l=0.4995, w1=0.049792708931209094, h1=0.049792708931209094, w2=0.0500595452386798, h2=0.0500595452386798, mleft=2.0,
mtop=2.0, mright=2.0, mbottom=2.0, alpha=3.044, G=-9.81, wavy=0.0057
)
AT (0.0, 0.0, 14.4255) RELATIVE e1_arm
ROTATED (0, 0, 0) RELATIVE e1_arm

COMPONENT E16_2 = Guide_gravity(
   l=0.4995, w1=0.0500595452386798, h1=0.0500595452386798, w2=0.05027807990249588, h2=0.05027807990249588, mleft=2.0, mtop=2.0,
mright=2.0, mbottom=2.0, alpha=3.044, G=-9.81, wavy=0.0057
)
AT (0.0, 0.0, 14.926) RELATIVE e1_arm
ROTATED (0, 0, 0) RELATIVE e1_arm

COMPONENT E16_3 = Guide_gravity(
   l=0.4995, w1=0.05027807990249588, h1=0.05027807990249588, w2=0.05044894062557809, h2=0.05044894062557809, mleft=1.5,
mtop=1.5, mright=1.5, mbottom=1.5, alpha=3.044, G=-9.81, wavy=0.0057
)
AT (0.0, 0.0, 15.4255) RELATIVE e1_arm
ROTATED (0, 0, 0) RELATIVE e1_arm

COMPONENT E16_4 = Guide_gravity(
   l=0.4995, w1=0.05044894062557809, h1=0.05044894062557809, w2=0.05057261061273639, h2=0.05057261061273639, mleft=1.5,
mtop=1.5, mright=1.5, mbottom=1.5, alpha=3.044, G=-9.81, wavy=0.0057
)
AT (0.0, 0.0, 15.926) RELATIVE e1_arm
ROTATED (0, 0, 0) RELATIVE e1_arm

COMPONENT E16_5 = Guide_gravity(
   l=0.4995, w1=0.05057261061273639, h1=0.05057261061273639, w2=0.05064943553994284, h2=0.05064943553994284, mleft=1.5,
mtop=1.5, mright=1.5, mbottom=1.5, alpha=3.044, G=-9.81, wavy=0.0057
)
AT (0.0, 0.0, 16.425500000000003) RELATIVE e1_arm
ROTATED (0, 0, 0) RELATIVE e1_arm

COMPONENT E16_6 = Guide_gravity(
   l=0.4995, w1=0.05064943553994284, h1=0.05064943553994284, w2=0.05067962844403265, h2=0.05067962844403265, mleft=1.5,
mtop=1.5, mright=1.5, mbottom=1.5, alpha=3.044, G=-9.81, wavy=0.0057
)
AT (0.0, 0.0, 16.926000000000002) RELATIVE e1_arm
ROTATED (0, 0, 0) RELATIVE e1_arm

COMPONENT TG1_0 = Guide_gravity(
   l=0.4995, w1=0.050680142255718985, h1=0.050680142255718985, w2=0.050680142255718985, h2=0.050680142255718985, mleft=1.5,
mtop=1.5, mright=1.5, mbottom=1.5, alpha=3.044, G=-9.81, wavy=0.0057
)
```

```
AT (0.0, 0.0, 17.425500000000003) RELATIVE e1_arm
ROTATED (0, 0, 0) RELATIVE e1_arm

COMPONENT TG1_1 = Guide_gravity(
   l=0.4995, w1=0.050680142255718985, h1=0.050680142255718985, w2=0.050680142255718985, h2=0.050680142255718985, mleft=1.5,
mtop=1.5, mright=1.5, mbottom=1.5, alpha=3.044, G=-9.81, wavy=0.0057
)
AT (0.0, 0.0, 17.926000000000002) RELATIVE e1_arm
ROTATED (0, 0, 0) RELATIVE e1_arm

COMPONENT TG1_2 = Guide_gravity(
   l=0.4995, w1=0.050680142255718985, h1=0.050680142255718985, w2=0.050680142255718985, h2=0.050680142255718985, mleft=1.5,
mtop=1.5, mright=1.5, mbottom=1.5, alpha=3.044, G=-9.81, wavy=0.0057
)
AT (0.0, 0.0, 18.425500000000003) RELATIVE e1_arm
ROTATED (0, 0, 0) RELATIVE e1_arm

COMPONENT TG1_3 = Guide_gravity(
   l=0.4995, w1=0.050680142255718985, h1=0.050680142255718985, w2=0.050680142255718985, h2=0.050680142255718985, mleft=1.5,
mtop=1.5, mright=1.5, mbottom=1.5, alpha=3.044, G=-9.81, wavy=0.0057
)
AT (0.0, 0.0, 18.926000000000002) RELATIVE e1_arm
ROTATED (0, 0, 0) RELATIVE e1_arm

COMPONENT TG1_4 = Guide_gravity(
   l=0.4995, w1=0.050680142255718985, h1=0.050680142255718985, w2=0.050680142255718985, h2=0.050680142255718985, mleft=1.5,
mtop=1.5, mright=1.5, mbottom=1.5, alpha=3.044, G=-9.81, wavy=0.0057
)
AT (0.0, 0.0, 19.425500000000003) RELATIVE e1_arm
ROTATED (0, 0, 0) RELATIVE e1_arm

COMPONENT TG1_5 = Guide_gravity(
   l=0.4995, w1=0.050680142255718985, h1=0.050680142255718985, w2=0.050680142255718985, h2=0.050680142255718985, mleft=1.5,
mtop=1.5, mright=1.5, mbottom=1.5, alpha=3.044, G=-9.81, wavy=0.0057
)
AT (0.0, 0.0, 19.926000000000002) RELATIVE e1_arm
ROTATED (0, 0, 0) RELATIVE e1_arm

COMPONENT TG1_6 = Guide_gravity(
   l=0.4995, w1=0.050680142255718985, h1=0.050680142255718985, w2=0.050680142255718985, h2=0.050680142255718985, mleft=1.5,
mtop=1.5, mright=1.5, mbottom=1.5, alpha=3.044, G=-9.81, wavy=0.0057
)
AT (0.0, 0.0, 20.425500000000003) RELATIVE e1_arm
ROTATED (0, 0, 0) RELATIVE e1_arm

COMPONENT TG1_7 = Guide_gravity(
   l=0.4995, w1=0.050680142255718985, h1=0.050680142255718985, w2=0.050680142255718985, h2=0.050680142255718985, mleft=1.5,
mtop=1.5, mright=1.5, mbottom=1.5, alpha=3.044, G=-9.81, wavy=0.0057
)
AT (0.0, 0.0, 20.926000000000002) RELATIVE e1_arm
ROTATED (0, 0, 0) RELATIVE e1_arm

COMPONENT TG1_8 = Guide_gravity(
   l=0.4995, w1=0.050680142255718985, h1=0.050680142255718985, w2=0.050680142255718985, h2=0.050680142255718985, mleft=1.5,
mtop=1.5, mright=1.5, mbottom=1.5, alpha=3.044, G=-9.81, wavy=0.0057
)
AT (0.0, 0.0, 21.425500000000003) RELATIVE e1_arm
ROTATED (0, 0, 0) RELATIVE e1_arm

COMPONENT TG1_9 = Guide_gravity(
   l=0.4995, w1=0.050680142255718985, h1=0.050680142255718985, w2=0.050680142255718985, h2=0.050680142255718985, mleft=1.5,
mtop=1.5, mright=1.5, mbottom=1.5, alpha=3.044, G=-9.81, wavy=0.0057
)
AT (0.0, 0.0, 21.926000000000002) RELATIVE e1_arm
ROTATED (0, 0, 0) RELATIVE e1_arm

COMPONENT TG1_10 = Guide_gravity(
   l=0.4995, w1=0.050680142255718985, h1=0.050680142255718985, w2=0.050680142255718985, h2=0.050680142255718985, mleft=1.5,
mtop=1.5, mright=1.5, mbottom=1.5, alpha=3.044, G=-9.81, wavy=0.0057
)
```

```
AT (0.0, 0.0, 22.425500000000003) RELATIVE e1_arm
ROTATED (0, 0, 0) RELATIVE e1_arm

COMPONENT TG1_11 = Guide_gravity(
   l=0.4995, w1=0.050680142255718985, h1=0.050680142255718985, w2=0.050680142255718985, h2=0.050680142255718985, mleft=1.5,
mtop=1.5, mright=1.5, mbottom=1.5, alpha=3.044, G=-9.81, wavy=0.0057
)
AT (0.0, 0.0, 22.926000000000002) RELATIVE e1_arm
ROTATED (0, 0, 0) RELATIVE e1_arm

COMPONENT TG1_12 = Guide_gravity(
   l=0.4995, w1=0.050680142255718985, h1=0.050680142255718985, w2=0.050680142255718985, h2=0.050680142255718985, mleft=1.0,
mtop=1.0, mright=1.0, mbottom=1.0, alpha=3.044, G=-9.81, wavy=0.0057
)
AT (0.0, 0.0, 23.425500000000003) RELATIVE e1_arm
ROTATED (0, 0, 0) RELATIVE e1_arm

COMPONENT TG1_13 = Guide_gravity(
   l=0.4995, w1=0.050680142255718985, h1=0.050680142255718985, w2=0.050680142255718985, h2=0.050680142255718985, mleft=1.0,
mtop=1.0, mright=1.0, mbottom=1.0, alpha=3.044, G=-9.81, wavy=0.0057
)
AT (0.0, 0.0, 23.926000000000002) RELATIVE e1_arm
ROTATED (0, 0, 0) RELATIVE e1_arm

COMPONENT TG1_14 = Guide_gravity(
   l=0.4995, w1=0.050680142255718985, h1=0.050680142255718985, w2=0.050680142255718985, h2=0.050680142255718985, mleft=1.0,
mtop=1.0, mright=1.0, mbottom=1.0, alpha=3.044, G=-9.81, wavy=0.0057
)
AT (0.0, 0.0, 24.425500000000003) RELATIVE e1_arm
ROTATED (0, 0, 0) RELATIVE e1_arm

COMPONENT pre_T0slit = PSD_monitor(
   nx=2, ny=2, xwidth=0.1, yheight=0.1, restore_neutron=1, filename="pre_T0slit.L"
)
AT (0.0, 0.0, 25.685000000000002) RELATIVE sample_arm
ROTATED (0, 0, 0) RELATIVE sample_arm

COMPONENT T0_slit = Slit(
   xwidth=0.046528, yheight=0.046528
)
AT (0.0, 0.0, 25.695000000000004) RELATIVE e1_arm
ROTATED (0, 0, 0) RELATIVE e1_arm

COMPONENT post_T0slit = PSD_monitor(
   nx=2, ny=2, xwidth=0.1, yheight=0.1, restore_neutron=1, filename="post_T0slit.L"
)
AT (0.0, 0.0, 25.705000000000005) RELATIVE sample_arm
ROTATED (0, 0, 0) RELATIVE sample_arm

COMPONENT TG2_0 = Guide_gravity(
   l=0.4995, w1=0.041972, h1=0.041972, w2=0.04197979166666667, h2=0.04197979166666667, mleft=1.0, mtop=1.0, mright=1.0,
mbottom=1.0, alpha=3.044, G=-9.81, wavy=0.0057
)
AT (0.0, 0.0, 26.834000000000003) RELATIVE e1_arm
ROTATED (0, 0, 0) RELATIVE e1_arm

COMPONENT TG2_1 = Guide_gravity(
   l=0.4995, w1=0.04197979166666667, h1=0.04197979166666667, w2=0.04200316666666667, h2=0.04200316666666667, mleft=1.0,
mtop=1.0, mright=1.0, mbottom=1.0, alpha=3.044, G=-9.81, wavy=0.0057
)
AT (0.0, 0.0, 27.333500000000004) RELATIVE e1_arm
ROTATED (0, 0, 0) RELATIVE e1_arm

COMPONENT TG2_2 = Guide_gravity(
   l=0.4995, w1=0.04200316666666667, h1=0.04200316666666667, w2=0.042042125, h2=0.042042125, mleft=1.0, mtop=1.0, mright=1.0,
mbottom=1.0, alpha=3.044, G=-9.81, wavy=0.0057
)
AT (0.0, 0.0, 27.834000000000003) RELATIVE e1_arm
ROTATED (0, 0, 0) RELATIVE e1_arm
```

```
COMPONENT TG2_3 = Guide_gravity(
   l=0.4995, w1=0.042042125, h1=0.042042125, w2=0.04209666666666667, h2=0.04209666666666667, mleft=1.0, mtop=1.0, mright=1.0,
mbottom=1.0, alpha=3.044, G=-9.81, wavy=0.0057
)
AT (0.0, 0.0, 28.333500000000004) RELATIVE e1_arm
ROTATED (0, 0, 0) RELATIVE e1_arm

COMPONENT TG2_4 = Guide_gravity(
   l=0.4995, w1=0.04209666666666667, h1=0.04209666666666667, w2=0.04216679166666667, h2=0.04216679166666667, mleft=1.0,
mtop=1.0, mright=1.0, mbottom=1.0, alpha=3.044, G=-9.81, wavy=0.0057
)
AT (0.0, 0.0, 28.834000000000003) RELATIVE e1_arm
ROTATED (0, 0, 0) RELATIVE e1_arm

COMPONENT TG2_5 = Guide_gravity(
   l=0.4995, w1=0.04216679166666667, h1=0.04216679166666667, w2=0.0422525, h2=0.0422525, mleft=1.0, mtop=1.0, mright=1.0,
mbottom=1.0, alpha=3.044, G=-9.81, wavy=0.0057
)
AT (0.0, 0.0, 29.333500000000004) RELATIVE e1_arm
ROTATED (0, 0, 0) RELATIVE e1_arm

COMPONENT TG2_6 = Guide_gravity(
   l=0.4995, w1=0.0422525, h1=0.0422525, w2=0.04235379166666667, h2=0.04235379166666667, mleft=1.0, mtop=1.0, mright=1.0,
mbottom=1.0, alpha=3.044, G=-9.81, wavy=0.0057
)
AT (0.0, 0.0, 29.834000000000003) RELATIVE e1_arm
ROTATED (0, 0, 0) RELATIVE e1_arm

COMPONENT TG2_7 = Guide_gravity(
   l=0.4995, w1=0.04235379166666667, h1=0.04235379166666667, w2=0.04247066666666667, h2=0.04247066666666667, mleft=1.0,
mtop=1.0, mright=1.0, mbottom=1.0, alpha=3.044, G=-9.81, wavy=0.0057
)
AT (0.0, 0.0, 30.333500000000004) RELATIVE e1_arm
ROTATED (0, 0, 0) RELATIVE e1_arm

COMPONENT TG2_8 = Guide_gravity(
   l=0.4995, w1=0.04247066666666667, h1=0.04247066666666667, w2=0.042603125, h2=0.042603125, mleft=1.5, mtop=1.5, mright=1.5,
mbottom=1.5, alpha=3.044, G=-9.81, wavy=0.0057
)
AT (0.0, 0.0, 30.834000000000003) RELATIVE e1_arm
ROTATED (0, 0, 0) RELATIVE e1_arm

COMPONENT TG2_9 = Guide_gravity(
   l=0.4995, w1=0.042603125, h1=0.042603125, w2=0.042751166666666666, h2=0.042751166666666666, mleft=1.5, mtop=1.5, mright=1.5,
mbottom=1.5, alpha=3.044, G=-9.81, wavy=0.0057
)
AT (0.0, 0.0, 31.333500000000004) RELATIVE e1_arm
ROTATED (0, 0, 0) RELATIVE e1_arm

COMPONENT TG2_10 = Guide_gravity(
   l=0.4995, w1=0.042751166666666666, h1=0.042751166666666666, w2=0.04291479166666667, h2=0.04291479166666667, mleft=1.5,
mtop=1.5, mright=1.5, mbottom=1.5, alpha=3.044, G=-9.81, wavy=0.0057
)
AT (0.0, 0.0, 31.834000000000003) RELATIVE e1_arm
ROTATED (0, 0, 0) RELATIVE e1_arm

COMPONENT TG2_11 = Guide_gravity(
   l=0.4995, w1=0.04291479166666667, h1=0.04291479166666667, w2=0.043094, h2=0.043094, mleft=1.5, mtop=1.5, mright=1.5,
mbottom=1.5, alpha=3.044, G=-9.81, wavy=0.0057
)
AT (0.0, 0.0, 32.3335) RELATIVE e1_arm
ROTATED (0, 0, 0) RELATIVE e1_arm

COMPONENT pre_VSslit = PSD_monitor(
   nx=2, ny=2, xwidth=0.1, yheight=0.1, restore_neutron=1, filename="pre_VSslit.L"
)
AT (0.0, 0.0, 33.9906) RELATIVE sample_arm
ROTATED (0, 0, 0) RELATIVE sample_arm

COMPONENT VS_slit = Slit(
```

```
   xwidth=0.040472, yheight=0.040472
)
AT (0.0, 0.0, 34.0006) RELATIVE e1_arm
ROTATED (0, 0, 0) RELATIVE e1_arm

COMPONENT post_VSslit = PSD_monitor(
   nx=2, ny=2, xwidth=0.1, yheight=0.1, restore_neutron=1, filename="post_VSslit.L"
)
AT (0.0, 0.0, 34.0106) RELATIVE sample_arm
ROTATED (0, 0, 0) RELATIVE sample_arm

COMPONENT TG3_0 = Guide_gravity(
   l=0.4995, w1=0.039297, h1=0.039297, w2=0.03984209259259259, h2=0.03984209259259259, mleft=1.5, mtop=1.5, mright=1.5,
mbottom=1.5, alpha=3.044, G=-9.81, wavy=0.0057
)
AT (0.0, 0.0, 34.5715) RELATIVE e1_arm
ROTATED (0, 0, 0) RELATIVE e1_arm

COMPONENT TG3_1 = Guide_gravity(
   l=0.4995, w1=0.03984209259259259, h1=0.03984209259259259, w2=0.04035603703703704, h2=0.04035603703703704, mleft=1.5,
mtop=1.5, mright=1.5, mbottom=1.5, alpha=3.044, G=-9.81, wavy=0.0057
)
AT (0.0, 0.0, 35.071) RELATIVE e1_arm
ROTATED (0, 0, 0) RELATIVE e1_arm

COMPONENT TG3_2 = Guide_gravity(
   l=0.4995, w1=0.04035603703703704, h1=0.04035603703703704, w2=0.04083883333333333, h2=0.04083883333333333, mleft=1.5,
mtop=1.5, mright=1.5, mbottom=1.5, alpha=3.044, G=-9.81, wavy=0.0057
)
AT (0.0, 0.0, 35.5715) RELATIVE e1_arm
ROTATED (0, 0, 0) RELATIVE e1_arm

COMPONENT TG3_3 = Guide_gravity(
   l=0.4995, w1=0.04083883333333333, h1=0.04083883333333333, w2=0.041290481481481484, h2=0.041290481481481484, mleft=1.5,
mtop=1.5, mright=1.5, mbottom=1.5, alpha=3.044, G=-9.81, wavy=0.0057
)
AT (0.0, 0.0, 36.071) RELATIVE e1_arm
ROTATED (0, 0, 0) RELATIVE e1_arm

COMPONENT TG3_4 = Guide_gravity(
   l=0.4995, w1=0.041290481481481484, h1=0.041290481481481484, w2=0.04171098148148148, h2=0.04171098148148148, mleft=1.5,
mtop=1.5, mright=1.5, mbottom=1.5, alpha=3.044, G=-9.81, wavy=0.0057
)
AT (0.0, 0.0, 36.5715) RELATIVE e1_arm
ROTATED (0, 0, 0) RELATIVE e1_arm

COMPONENT TG3_5 = Guide_gravity(
   l=0.4995, w1=0.04171098148148148, h1=0.04171098148148148, w2=0.04210033333333333, h2=0.04210033333333333, mleft=1.5,
mtop=1.5, mright=1.5, mbottom=1.5, alpha=3.044, G=-9.81, wavy=0.0057
)
AT (0.0, 0.0, 37.071) RELATIVE e1_arm
ROTATED (0, 0, 0) RELATIVE e1_arm

COMPONENT TG3_6 = Guide_gravity(
   l=0.4995, w1=0.04210033333333333, h1=0.04210033333333333, w2=0.04245853703703704, h2=0.04245853703703704, mleft=1.5,
mtop=1.5, mright=1.5, mbottom=1.5, alpha=3.044, G=-9.81, wavy=0.0057
)
AT (0.0, 0.0, 37.5715) RELATIVE e1_arm
ROTATED (0, 0, 0) RELATIVE e1_arm

COMPONENT TG3_7 = Guide_gravity(
   l=0.4995, w1=0.04245853703703704, h1=0.04245853703703704, w2=0.04278559259259259, h2=0.04278559259259259, mleft=1.5,
mtop=1.5, mright=1.5, mbottom=1.5, alpha=3.044, G=-9.81, wavy=0.0057
)
AT (0.0, 0.0, 38.071) RELATIVE e1_arm
ROTATED (0, 0, 0) RELATIVE e1_arm

COMPONENT TG3_8 = Guide_gravity(
   l=0.4995, w1=0.04278559259259259, h1=0.04278559259259259, w2=0.0430815, h2=0.0430815, mleft=1.5, mtop=1.5, mright=1.5,
mbottom=1.5, alpha=3.044, G=-9.81, wavy=0.0057
```

```
)
AT (0.0, 0.0, 38.5715) RELATIVE e1_arm
ROTATED (0, 0, 0) RELATIVE e1_arm

COMPONENT TG3_9 = Guide_gravity(
   l=0.4995, w1=0.0430815, h1=0.0430815, w2=0.04334625925925926, h2=0.04334625925925926, mleft=1.5, mtop=1.5, mright=1.5,
mbottom=1.5, alpha=3.044, G=-9.81, wavy=0.0057
)
AT (0.0, 0.0, 39.071) RELATIVE e1_arm
ROTATED (0, 0, 0) RELATIVE e1_arm

COMPONENT TG3_10 = Guide_gravity(
   l=0.4995, w1=0.04334625925925926, h1=0.04334625925925926, w2=0.04357987037037037, h2=0.04357987037037037, mleft=1.5,
mtop=1.5, mright=1.5, mbottom=1.5, alpha=3.044, G=-9.81, wavy=0.0057
)
AT (0.0, 0.0, 39.5715) RELATIVE e1_arm
ROTATED (0, 0, 0) RELATIVE e1_arm

COMPONENT TG3_11 = Guide_gravity(
   l=0.4995, w1=0.04357987037037037, h1=0.04357987037037037, w2=0.04378233333333333, h2=0.04378233333333333, mleft=1.5,
mtop=1.5, mright=1.5, mbottom=1.5, alpha=3.044, G=-9.81, wavy=0.0057
)
AT (0.0, 0.0, 40.071) RELATIVE e1_arm
ROTATED (0, 0, 0) RELATIVE e1_arm

COMPONENT TG3_12 = Guide_gravity(
   l=0.4995, w1=0.04378233333333333, h1=0.04378233333333333, w2=0.043953648148148144, h2=0.043953648148148144, mleft=1.5,
mtop=1.5, mright=1.5, mbottom=1.5, alpha=3.044, G=-9.81, wavy=0.0057
)
AT (0.0, 0.0, 40.5715) RELATIVE e1_arm
ROTATED (0, 0, 0) RELATIVE e1_arm

COMPONENT TG3_13 = Guide_gravity(
   l=0.4995, w1=0.043953648148148144, h1=0.043953648148148144, w2=0.044093814814814815, h2=0.044093814814814815, mleft=1.5,
mtop=1.5, mright=1.5, mbottom=1.5, alpha=3.044, G=-9.81, wavy=0.0057
)
AT (0.0, 0.0, 41.071) RELATIVE e1_arm
ROTATED (0, 0, 0) RELATIVE e1_arm

COMPONENT TG3_14 = Guide_gravity(
   l=0.4995, w1=0.044093814814814815, h1=0.044093814814814815, w2=0.04420283333333334, h2=0.04420283333333334, mleft=1.5,
mtop=1.5, mright=1.5, mbottom=1.5, alpha=3.044, G=-9.81, wavy=0.0057
)
AT (0.0, 0.0, 41.5715) RELATIVE e1_arm
ROTATED (0, 0, 0) RELATIVE e1_arm

COMPONENT TG3_15 = Guide_gravity(
   l=0.4995, w1=0.04420283333333334, h1=0.04420283333333334, w2=0.044280703703703704, h2=0.044280703703703704, mleft=1.5,
mtop=1.5, mright=1.5, mbottom=1.5, alpha=3.044, G=-9.81, wavy=0.0057
)
AT (0.0, 0.0, 42.071) RELATIVE e1_arm
ROTATED (0, 0, 0) RELATIVE e1_arm

COMPONENT TG3_16 = Guide_gravity(
   l=0.4995, w1=0.044280703703703704, h1=0.044280703703703704, w2=0.04432742592592592, h2=0.04432742592592592, mleft=1.5,
mtop=1.5, mright=1.5, mbottom=1.5, alpha=3.044, G=-9.81, wavy=0.0057
)
AT (0.0, 0.0, 42.5715) RELATIVE e1_arm
ROTATED (0, 0, 0) RELATIVE e1_arm

COMPONENT TG3_17 = Guide_gravity(
   l=0.4995, w1=0.04432742592592592, h1=0.04432742592592592, w2=0.044343, h2=0.044343, mleft=1.5, mtop=1.5, mright=1.5,
mbottom=1.5, alpha=3.044, G=-9.81, wavy=0.0057
)
AT (0.0, 0.0, 43.071) RELATIVE e1_arm
ROTATED (0, 0, 0) RELATIVE e1_arm

COMPONENT E21_0 = Guide_gravity(
   l=0.4995, w1=0.037799295889665206, h1=0.037799295889665206, w2=0.037687370277061774, h2=0.037687370277061774, mleft=1.5,
mtop=1.5, mright=1.5, mbottom=1.5, alpha=3.044, G=-9.81, wavy=0.0057
```

```
)
AT (0.0, 0.0, 45.4645) RELATIVE e1_arm
ROTATED (0, 0, 0) RELATIVE e1_arm

COMPONENT E21_1 = Guide_gravity(
   l=0.4995, w1=0.037687370277061774, h1=0.037687370277061774, w2=0.03749632053023786, h2=0.03749632053023786, mleft=1.5,
mtop=1.5, mright=1.5, mbottom=1.5, alpha=3.044, G=-9.81, wavy=0.0057
)
AT (0.0, 0.0, 45.964) RELATIVE e1_arm
ROTATED (0, 0, 0) RELATIVE e1_arm

COMPONENT E21_2 = Guide_gravity(
   l=0.4995, w1=0.03749632053023786, h1=0.03749632053023786, w2=0.037224928401172176, h2=0.037224928401172176, mleft=1.5,
mtop=1.5, mright=1.5, mbottom=1.5, alpha=3.044, G=-9.81, wavy=0.0057
)
AT (0.0, 0.0, 46.4645) RELATIVE e1_arm
ROTATED (0, 0, 0) RELATIVE e1_arm

COMPONENT E21_3 = Guide_gravity(
   l=0.4995, w1=0.037224928401172176, h1=0.037224928401172176, w2=0.036871419851946745, h2=0.036871419851946745, mleft=1.5,
mtop=1.5, mright=1.5, mbottom=1.5, alpha=3.044, G=-9.81, wavy=0.0057
)
AT (0.0, 0.0, 46.964) RELATIVE e1_arm
ROTATED (0, 0, 0) RELATIVE e1_arm

COMPONENT E21_4 = Guide_gravity(
   l=0.4995, w1=0.036871419851946745, h1=0.036871419851946745, w2=0.036433404666387545, h2=0.036433404666387545, mleft=1.5,
mtop=1.5, mright=1.5, mbottom=1.5, alpha=3.044, G=-9.81, wavy=0.0057
)
AT (0.0, 0.0, 47.4645) RELATIVE e1_arm
ROTATED (0, 0, 0) RELATIVE e1_arm

COMPONENT E21_5 = Guide_gravity(
   l=0.4995, w1=0.036433404666387545, h1=0.036433404666387545, w2=0.03590779045737912, h2=0.03590779045737912, mleft=1.5,
mtop=1.5, mright=1.5, mbottom=1.5, alpha=3.044, G=-9.81, wavy=0.0057
)
AT (0.0, 0.0, 47.964) RELATIVE e1_arm
ROTATED (0, 0, 0) RELATIVE e1_arm

COMPONENT E21_6 = Guide_gravity(
   l=0.4995, w1=0.03590779045737912, h1=0.03590779045737912, w2=0.035290663379106725, h2=0.035290663379106725, mleft=1.5,
mtop=1.5, mright=1.5, mbottom=1.5, alpha=3.044, G=-9.81, wavy=0.0057
)
AT (0.0, 0.0, 48.4645) RELATIVE e1_arm
ROTATED (0, 0, 0) RELATIVE e1_arm

COMPONENT E21_7 = Guide_gravity(
   l=0.4995, w1=0.035290663379106725, h1=0.035290663379106725, w2=0.03457712385673339, h2=0.03457712385673339, mleft=1.5,
mtop=1.5, mright=1.5, mbottom=1.5, alpha=3.044, G=-9.81, wavy=0.0057
)
AT (0.0, 0.0, 48.964) RELATIVE e1_arm
ROTATED (0, 0, 0) RELATIVE e1_arm

COMPONENT E21b_0 = Guide_gravity(
   l=0.4995, w1=0.03457712385673339, h1=0.03457712385673339, w2=0.03376105941658848, h2=0.03376105941658848, mleft=1.5,
mtop=1.5, mright=1.5, mbottom=1.5, alpha=3.044, G=-9.81, wavy=0.0057
)
AT (0.0, 0.0, 49.4645) RELATIVE e1_arm
ROTATED (0, 0, 0) RELATIVE e1_arm

COMPONENT E21b_1 = Guide_gravity(
   l=0.4995, w1=0.03376105941658848, h1=0.03376105941658848, w2=0.0328348266009893, h2=0.0328348266009893, mleft=1.5, mtop=1.5,
mright=1.5, mbottom=1.5, alpha=3.044, G=-9.81, wavy=0.0057
)
AT (0.0, 0.0, 49.964) RELATIVE e1_arm
ROTATED (0, 0, 0) RELATIVE e1_arm

COMPONENT E21b_2 = Guide_gravity(
   l=0.4995, w1=0.0328348266009893, h1=0.0328348266009893, w2=0.03178879691280767, h2=0.03178879691280767, mleft=2.0, mtop=2.0,
mright=2.0, mbottom=2.0, alpha=3.044, G=-9.81, wavy=0.0057
```

```
)
AT (0.0, 0.0, 50.4645) RELATIVE e1_arm
ROTATED (0, 0, 0) RELATIVE e1_arm

COMPONENT E21b_3 = Guide_gravity(
   l=0.4995, w1=0.03178879691280767, h1=0.03178879691280767, w2=0.03061069170519521, h2=0.03061069170519521, mleft=2.0,
mtop=2.0, mright=2.0, mbottom=2.0, alpha=3.044, G=-9.81, wavy=0.0057
)
AT (0.0, 0.0, 50.964) RELATIVE e1_arm
ROTATED (0, 0, 0) RELATIVE e1_arm

COMPONENT E21b_4 = Guide_gravity(
   l=0.4995, w1=0.03061069170519521, h1=0.03061069170519521, w2=0.029284575298907153, h2=0.029284575298907153, mleft=2.0,
mtop=2.0, mright=2.0, mbottom=2.0, alpha=3.044, G=-9.81, wavy=0.0057
)
AT (0.0, 0.0, 51.4645) RELATIVE e1_arm
ROTATED (0, 0, 0) RELATIVE e1_arm

COMPONENT E21b_5 = Guide_gravity(
   l=0.4995, w1=0.029284575298907153, h1=0.029284575298907153, w2=0.02778926628150335, h2=0.02778926628150335, mleft=2.0,
mtop=2.0, mright=2.0, mbottom=2.0, alpha=3.044, G=-9.81, wavy=0.0057
)
AT (0.0, 0.0, 51.964) RELATIVE e1_arm
ROTATED (0, 0, 0) RELATIVE e1_arm

COMPONENT E21b_6 = Guide_gravity(
   l=0.4995, w1=0.02778926628150335, h1=0.02778926628150335, w2=0.026095696134637116, h2=0.026095696134637116, mleft=2.5,
mtop=2.5, mright=2.5, mbottom=2.5, alpha=3.044, G=-9.81, wavy=0.0057
)
AT (0.0, 0.0, 52.4645) RELATIVE e1_arm
ROTATED (0, 0, 0) RELATIVE e1_arm

COMPONENT E21b_7 = Guide_gravity(
   l=0.4995, w1=0.026095696134637116, h1=0.026095696134637116, w2=0.024162211390897373, h2=0.024162211390897373, mleft=2.5,
mtop=2.5, mright=2.5, mbottom=2.5, alpha=3.044, G=-9.81, wavy=0.0057
)
AT (0.0, 0.0, 52.964) RELATIVE e1_arm
ROTATED (0, 0, 0) RELATIVE e1_arm

COMPONENT E21c_0 = Guide_gravity(
   l=0.4995, w1=0.024162211390897373, h1=0.024162211390897373, w2=0.021925433361865077, h2=0.021925433361865077, mleft=2.5,
mtop=2.5, mright=2.5, mbottom=2.5, alpha=3.044, G=-9.81, wavy=0.0057
)
AT (0.0, 0.0, 53.4645) RELATIVE e1_arm
ROTATED (0, 0, 0) RELATIVE e1_arm

COMPONENT E21c_1 = Guide_gravity(
   l=0.4995, w1=0.021925433361865077, h1=0.021925433361865077, w2=0.0192800898123645, h2=0.0192800898123645, mleft=2.5,
mtop=2.5, mright=2.5, mbottom=2.5, alpha=3.044, G=-9.81, wavy=0.0057
)
AT (0.0, 0.0, 53.964) RELATIVE e1_arm
ROTATED (0, 0, 0) RELATIVE e1_arm

COMPONENT pre_E2aslit = PSD_monitor(
   nx=2, ny=2, xwidth=0.1, yheight=0.1, restore_neutron=1, filename="pre_E2aslit.L"
)
AT (0.0, 0.0, 54.569500000000005) RELATIVE sample_arm
ROTATED (0, 0, 0) RELATIVE sample_arm

COMPONENT E2_slita = Slit(
   xwidth=0.019833, yheight=0.019833
)
AT (0.0, 0.0, 54.5795) RELATIVE e1_arm
ROTATED (0, 0, 0) RELATIVE e1_arm

COMPONENT post_E2aslit = PSD_monitor(
   nx=2, ny=2, xwidth=0.1, yheight=0.1, restore_neutron=1, filename="post_E2aslit.L"
)
AT (0.0, 0.0, 54.5895) RELATIVE sample_arm
ROTATED (0, 0, 0) RELATIVE sample_arm
```

```
COMPONENT pre_sizeslit = PSD_monitor(
   nx=2, ny=2, xwidth=0.1, yheight=0.1, restore_neutron=1, filename="pre_sizeslit.L"
)
AT (0.0, 0.0, 55.3604) RELATIVE sample_arm
ROTATED (0, 0, 0) RELATIVE sample_arm

COMPONENT Size_slit = Slit(
   xwidth=0.011972, yheight=0.011972
)
AT (0.0, 0.0001, 55.3704) RELATIVE e1_arm
ROTATED (0, 0, 0) RELATIVE e1_arm

COMPONENT post_sizeslit = PSD_monitor(
   nx=2, ny=2, xwidth=0.1, yheight=0.1, restore_neutron=1, filename="post_sizeslit.L"
)
AT (0.0, 0.0, 55.380399999999995) RELATIVE sample_arm
ROTATED (0, 0, 0) RELATIVE sample_arm

COMPONENT Final_aperature = Slit(
   xwidth=0.0068754, yheight=0.0068754
)
AT (0.0, 0.0001, 55.8) RELATIVE e1_arm
ROTATED (0, 0, 0) RELATIVE e1_arm

COMPONENT Mask = Slit(
   xwidth=0.02, yheight=0.02
)
AT (0.0, 0.0, 0.0) RELATIVE sample_arm
ROTATED (0, 0, 0) RELATIVE sample_arm

COMPONENT neutron_at_sample = MCPL_output(
   filename="neutrons_at_sample"
)
AT (0, 0, 1e-05) RELATIVE sample_arm


FINALLY
%{
%}
END
```

REFERENCE

1. Carpenter, J.M. and C.-K. Loong, *Elements of slow-neutron scattering*. 2015: Cambridge University Press.
2. Bullock, M. and K. More, *Basic Energy Sciences Roundtable: Foundational Science for Carbon-Neutral Hydrogen Technologies (Report)*. 2022, DOESC Office of Basic Energy Sciences.
3. *Basic Energy Sciences Roundtable: Foundational Science for Carbon Dioxide Removal Technologies (Brochure)*. 2022: United States. p. Medium: ED; Size: 4 p.
4. Murray, C., et al., *Basic Research Needs for Microelectronics: Report of the Office of Science Workshop on Basic Research Needs for Microelectronics, October 23–25, 2018*. 2018, USDOE Office of Science (SC)(United States).
5. Broholm, C., et al., *Basic research needs workshop on quantum materials for energy relevant technology*. 2016, USDOE Office of Science (SC)(United States).
6. Hemminger, J.C., et al., *Challenges at the frontiers of matter and energy: Transformative opportunities for discovery science*. 2015, USDOE Office of Science (SC)(United States).
7. Adams, P., et al., *First Experiments: New Science Opportunities at the Spallation Neutron Source Second Target Station (abridged)*. 2020: United States. p. Medium: ED; Size: 19 p.
8. Liu, Y., et al., *PIONEER, a high-resolution single-crystal polarized neutron diffractometer.* Review of Scientific Instruments, 2022. **93**(7).
9. Dhayal, R.S., et al., *Diselenophosphate-induced conversion of an achiral [Cu20H11 {S2P (OiPr) 2} 9] into a chiral [Cu20H11 {Se2P (OiPr) 2} 9] polyhydrido nanocluster.* Angewandte Chemie International Edition, 2015. **54**(46): p. 13604-13608.
10. Peterson, P.F., et al., *Event-based processing of neutron scattering data.* Nuclear Instruments and Methods in Physics Research Section A: Accelerators, Spectrometers, Detectors and Associated Equipment, 2015. **803**: p. 24-28.
11. Willendrup, P.K. and K. Lefmann, *McStas (i): Introduction, use, and basic principles for ray-tracing simulations.* Journal of Neutron Research, 2020. **22**(1): p. 1-16.
12. Willendrup, P.K. and K. Lefmann, *McStas (ii): An overview of components, their use, and advice for user contributions.* Journal of Neutron Research, 2021. **23**(1): p. 7-27.
13. Lin, J.Y., et al., *Recent developments of MCViNE and its applications at SNS.* Journal of Physics Communications, 2019. **3**(8): p. 085005.
14. Lin, J.Y., et al., *MCViNE–An object oriented Monte Carlo neutron ray tracing simulation package.* Nuclear Instruments and Methods in Physics Research Section A: Accelerators, Spectrometers, Detectors and Associated Equipment, 2016. **810**: p. 86-99.
15. Virtanen, P., et al., *SciPy 1.0: fundamental algorithms for scientific computing in Python.* Nature methods, 2020. **17**(3): p. 261-272.
16. Kluyver, T., et al., *Jupyter Notebooks-a publishing format for reproducible computational workflows.* Elpub, 2016. **2016**: p. 87-90.
17. Fitzsimmons, M. and C. Majkrzak, *Application of polarized neutron reflectometry to studies of artificially structured magnetic materials.* Modern techniques for characterizing magnetic materials, 2005: p. 1-52.
18. Seo, P.-N., et al., *High-efficiency resonant rf spin rotator with broad phase space acceptance for pulsed polarized cold neutron beams.* Physical Review Special Topics-Accelerators and Beams, 2008. **11**(8): p. 084701.
19. Stone, M.B., et al. *The ARCS radial collimator*. in *EPJ Web of Conferences*. 2015. EDP Sciences.
20. Haberl, B., et al., *3D-printed B4C collimation for neutron pressure cells.* Review of Scientific Instruments, 2021. **92**(9).
21. Islam, F., et al., *Computational optimization of a 3D printed collimator.* Journal of Neutron Research, 2020. **22**(2-3): p. 155-168.

22. Copley, J. and J. Cook, *An analysis of the effectiveness of oscillating radial collimators in neutron scattering applications.* Nuclear Instruments and Methods in Physics Research Section A: Accelerators, Spectrometers, Detectors and Associated Equipment, 1994. **345**(2): p. 313-323.
23. Nakamura, M., et al., *Performances of oscillating radial collimator for the Fermi chopper spectrometer 4SEASONS at J-PARC.* Physica B: Condensed Matter, 2018. **551**: p. 480-483.
24. Riedel, R., et al., *Design and performance of a large area neutron sensitive anger camera.* Nuclear Instruments and Methods in Physics Research Section A: Accelerators, Spectrometers, Detectors and Associated Equipment, 2015. **794**: p. 224-233.
25. Lazo, E.O., et al., *Robotic sample changers for macromolecular X-ray crystallography and biological small-angle X-ray scattering at the National Synchrotron Light Source II.* Journal of synchrotron radiation, 2021. **28**(5): p. 1649-1661.
26. Kornegay, F., *Spallation neutron source final safety assessment document for neutron facilities*. 2006, SNS Document Number.
27. Zendler, C., D.M. Rodriguez, and P. Bentley, *Generic guide concepts for the European Spallation Source.* Nuclear Instruments and Methods in Physics Research Section A: Accelerators, Spectrometers, Detectors and Associated Equipment, 2015. **803**: p. 89-99.
28. Mildner, D., *Acceptance diagrams for curved neutron guides.* Nuclear Instruments and Methods in Physics Research Section A: Accelerators, Spectrometers, Detectors and Associated Equipment, 1990. **290**(1): p. 189-196.
29. Schanzer, C., et al., *Advanced geometries for ballistic neutron guides.* Nuclear Instruments and Methods in Physics Research Section A: Accelerators, Spectrometers, Detectors and Associated Equipment, 2004. **529**(1-3): p. 63-68.
30. Zendler, C., D. Nekrassov, and K. Lieutenant, *An improved elliptic guide concept for a homogeneous neutron beam without direct line of sight.* Nuclear Instruments and Methods in Physics Research Section A: Accelerators, Spectrometers, Detectors and Associated Equipment, 2014. **746**: p. 39-46.
31. Jauch, W., *Prospects of single-crystal diffraction at a long pulse spallation source.* Journal of Neutron Research, 1997. **6**(1-3): p. 161-171.
32. Lin, J.Y., et al., *A realistic guide misalignment model for the Second Target Station instruments at the Spallation Neutron Source.* Nuclear Instruments and Methods in Physics Research Section A: Accelerators, Spectrometers, Detectors and Associated Equipment, 2023. **1047**: p. 167881.
33. Hansen, U.B., et al., *Simulation of waviness in neutron guides.* Journal of Neutron Research, 2015. **18**(2-3): p. 45-59.